

# Water Resources Research®

## RESEARCH ARTICLE

10.1029/2022WR032512

## Uncertainty Quantification of Transient-Based Leakage Identification: A Frequency Domain Framework

Huan-Feng Duan<sup>1</sup>  and Alireza Keramat<sup>1</sup> 

<sup>1</sup>Department of Civil and Environmental Engineering, The Hong Kong Polytechnic University, Hong Kong, China

### Key Points:

- Analytical formulations are offered to quantify the frequency-based leak detection uncertainty subjected to Gaussian measurements
- An in-depth analysis of leak signatures on limited bandwidth probing waves demonstrates the points of minimum errors in each pipeline
- Error-estimation graphs are recommended as valuable supplements to quantify the accuracy and efficiency of the leak detection exercise

### Correspondence to:

A. Keramat,  
alireza.keramat@polyu.edu.hk

### Citation:

Duan, H.-F., & Keramat, A. (2022). Uncertainty quantification of transient-based leakage identification: A frequency domain framework. *Water Resources Research*, 58, e2022WR032512. <https://doi.org/10.1029/2022WR032512>

Received 7 APR 2022  
Accepted 31 OCT 2022

### Author Contributions:

**Conceptualization:** Alireza Keramat  
**Formal analysis:** Alireza Keramat  
**Funding acquisition:** Huan-Feng Duan  
**Investigation:** Alireza Keramat  
**Methodology:** Alireza Keramat  
**Resources:** Huan-Feng Duan  
**Software:** Alireza Keramat  
**Supervision:** Alireza Keramat  
**Validation:** Alireza Keramat  
**Visualization:** Alireza Keramat  
**Writing – original draft:** Alireza Keramat  
**Writing – review & editing:** Huan-Feng Duan, Alireza Keramat

**Abstract** The leak detection methods in the frequency domain have presently become widely established among transient-based techniques. This study quantifies the uncertainty of the frequency domain multiple leak detection subjected to uncertain Gaussian, independent, and identically distributed measurements. The lower limit of the variances and covariances of the estimated leak locations and sizes are derived via the Cramer-Rao Lower Bound theory, whose derivation consistency with the Taylor expansion is also revealed. A systematic methodology based on the Monte Carlo simulations and probing waves is carried out to examine and verify the proposed formulations and corresponding outcomes, leading to an in-depth analysis of interactions between probing waves and leaks. The results justify the formation of points of minimum error in the pipeline corresponding to each specific harmonic wave, which has direct application in detectability using signals of limited bandwidth in actual practice. The findings resolve the reason behind localization failure for some test cases and success for others despite the same noise levels, as illustrated via numerical and experimental test cases. A workflow for efficient leak detection and the approach to estimating the corresponding localization uncertainty is proposed. According to the findings of this study, one may recommend the predicted error-location results to accompany the wave-based leak detection outputs to render a measure of accuracy in the identification process.

**Plain Language Summary** This article suggests a statistical framework for transient-based leak detection (TBLD) uncertainty quantification in the frequency domain. The key novelties and contributions of this perusal are twofold. (a) A robust framework for quantifying the leak detection uncertainty owing to the randomness of measurements is developed. It answers several unresolved questions in spectral-based leak detection, for example, correlation and variance of estimated quantities, required signal bandwidth to arrive at a specific accuracy, localization dependency to the actual location of leaks, and their interactions with standing waves. (b) It is demonstrated that the proposed uncertainty estimation graphs can supplement the localization results, thereby offering a solid theoretical tool to quantify the level of accuracy one may achieve in the leak detection practice. This study is significant to the authors' view as it overviews all TBLD methods in the frequency domain and resolves several relevant questions.

## 1. Introduction

Leakage from water distribution systems results in several negative consequences, including revenue loss and environmental and health concerns. Thus, various localization technologies have been developed. The transient-based leak detection (TBLD) has been recently received much attention due to its low cost, less intrusive process, and successful experiences in laboratory and field practice (e.g., Brunone, 1999; Che et al., 2021; Colombo et al., 2009; Covas & Ramos, 2010; Kapelan et al., 2003; Meniconi et al., 2021). One may categorize the TBLD methods into time, and frequency domain approaches, given the model solvers they incorporate in the estimation process. The so-called reflectometry or transient reflection method (e.g., Brunone et al., 2008), the inverse transient analysis (e.g., Kapelan et al., 2003; Keramat et al., 2019; Liggett & Chen, 1994; Malekpour & She, 2021; Soares et al., 2011; Vítkovský et al., 2007), the transient damping method (e.g., Asada et al., 2020; Covas & Ramos, 2010; X.-J. Wang et al., 2002) are identified as significant contributions in the time domain. On the other hand, the frequency response approach uses the frequency domain solution of pipe flow transients and enables comparisons with measured frequencies and corresponding amplitudes (e.g., Ferrante et al., 2016; Lee et al., 2013, 2015, 2005; Mpesha, 2011; Pan et al., 2021). As the TBLD approach is settled, methodologies to enhance and improve it are growing (e.g., Duan, 2017, 2018; Ferrante et al., 2007, 2016), and at the same time, techniques to assess the methods and report on the best possible detectability performance are sought (e.g., Ferrante et al., 2014; Keramat et al., 2019; Vítkovský et al., 2003; Zhang et al., 2020).

In the context of the transient pipe flows, the uncertainty quantification may be categorized in forward and inverse classes. The former seeks to estimate the uncertainty of the state variables subject to uncertain system parameters (including leaks), like the studies by Duan (2016), Ferrante et al. (2016), Sattar and El-Beltagy (2017), and X. Wang (2021). The inverse uncertainty quantification corresponds to the error bounds of the unknown parameters (such as the leak sizes and locations) when some state variables are measured. Since the inverse analysis comprises a computational model solver and a set of collected data, the uncertainty of the estimated parameters is dictated by the incorporated model and measurements. The uncertainties of the TBLD methods can be categorized into (a) the epistemic or modeling error, which deals with inaccuracies of the input parameters and governing equations and, (b) the aleatoric or statistical uncertainties on measured data such as environmental noise, instrument inaccuracies, turbulence, and air bubbles (X. Wang et al., 2020, Keramat et al., 2021). The latter may be assumed (or adjusted) to be i.i.d and Gaussian in the TBLD process. The present study estimates how much this measurement uncertainty can skew the leak detection results obtained from the frequency domain methods.

Considering the two classes of the TBLD, that is, time and frequency domain, the uncertainty evaluation of the leak parameters can also be divided into time and frequency domain methods. The estimation error in the time domain has been pioneered by Vítkovský et al. (2003), in which performance indicators to decide the optimal measurement locations in pipe networks were defined. Recently, Zhang et al. (2019, 2020) investigated the parameter uncertainties associated with the pipe wall condition, and Keramat et al. (2019) quantified the lower bound error of the estimated leak sizes. These studies found the connection between the resolution, valve maneuver, sensor placement, signal length, and the measurement noise level in a time domain framework. In comparison, the current study focuses on the frequency response formulations.

Essentially, the identification of defects based on transient data is a random process because of the wide range of uncertainties (measurements, wave speed, friction factor, mechanical properties of the pipeline and its structural supports, etc.) of the input data (Duan, 2016; Ferrante et al., 2016; Keramat & Zanganeh, 2019; Sattar & El-Beltagy, 2017; X. Wang, 2021; Zanganeh et al., 2020; Zhang et al., 2020). That means the result of the defect detection problem seeks to infer the parameters of a distribution (Casella & Berger, 2002). To date, the majority of defect detection studies have just focused on a single parameter of the distribution, that is, the mean. Nevertheless, the estimation variance contributes to an equivalent or sometimes more value (than the mean) in a stochastic context. The covariance matrix of the estimated quantities is among the significant parameters of a distribution that reports the error or variance of the leak unknowns and the correlation between them (off-diagonal elements of the covariance matrix; e.g., Keramat et al., 2019; Nehorai & Hawkes, 2000). Thus, the derivation and the investigation of the covariance matrix of the leak data is the objective of this research. In this context, Alawadhi and Tartakovsky (2020) used the Bayesian modeling to for the localization and its uncertainty quantification, but their approach is in the time domain, considered the initial conditions uncertainties, is computationally expensive, and limited to a single leak.

This research evaluates the lower bound of the leak parameters covariance matrix, or equivalently, the mean square error of the estimated leak sizes and locations. This estimation is accomplished based on the Fisher information matrix in a frequency domain framework, while Keramat et al. (2018) conducted it on a time-domain basis. The formulations are verified by the Monte Carlo method applied to the recent localization method developed by the authors (Keramat & Duan, 2021; Keramat et al., 2022). The analytical CRLB derivations allow for assessing localization techniques, and estimating the uncertainties of the leak sizes and locations as a supplemental report in the real practice of leak detection, as detailed via several case studies.

The rest of this research is organized as follows. First, the CRLB theory is applied to find the lower bound of the leak parameters covariance matrix. Then, the state formulation in a pipeline with multiple leaks is presented to enable computing the elements of the covariance matrix. The proposed formulations are then used in some numerical examples, and their results are comprehensively discussed. The computational investigations cover an in-depth analysis of the localization uncertainty, and an efficient leakage identification algorithm, followed by two experimental case studies. Concluding remarks on the CRLB application to the leakage identification uncertainty is finally drawn.

## 2. Problem Statement

In the frequency domain-based localization framework using some sets of collected transient signals, measurement uncertainties spread to the identified parameters. Therein, the following questions are crucial but have not received enough attention.

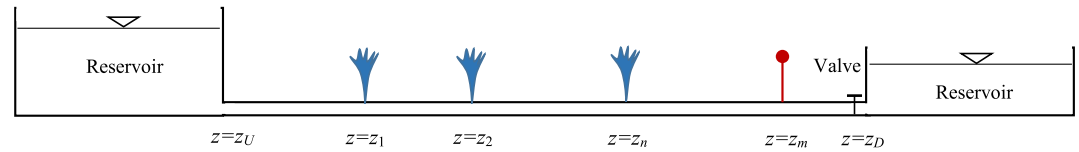


**Figure 1.** The schematic of the pipeline in a typical reservoir-multiple-leak-pipeline-valve system considered for the proposed uncertainty analysis and leak identification.

1. How many resonant frequencies (what signal bandwidth) is necessary to extract from the experimental data to arrive at a specific accuracy in localization? The need to find the appropriate number of resonant frequencies from the noisy data is grounded on two facts. First, in the transients frequency spectrum, the noise level increases at higher frequencies (e.g., X. Wang, Lin, et al., 2019; X. Wang, Palomar, et al., 2019) so that signals with higher bandwidths incorporate more noise in the localization process. That means exploiting high-bandwidth noisy signals in the leak location/size estimation cannot always be beneficial. Second, the wave-leak reflection theories (Louati et al., 2020) revealed that some waves are extremely sensitive to specific leak locations, thus significantly contributing to the localization of that leak. Based on the two facts, one can conclude that depending upon the leak location, a specific number of resonant frequencies are required and are enough to be incorporated in the localization process. More than that leads to skew the results because of the noise involvement from the later resonant frequencies.
2. What are the uncertainties corresponding to the identified leak sizes and locations? That is to say, how can the covariance matrix of the unknown leak parameters be quantified? The uncertainties here refer to the variance (standard deviation) of the leak locations and sizes and their correlations, which are less discussed in the literature.
3. Why can some leaks be conveniently localized and others not despite applying the same signal bandwidths? This question may be posed differently regarding the leak-wave interaction studied by Louati et al. (2020): why are some waves (frequencies) more vulnerable to noise and some less when used in detecting specific leaks?

The three questions are approached via quantifying the lower bound of the localization results, which implies the minimum of the covariance matrix (CRLB) for a given set of system parameters and transient signals. More precisely, the CRLB of  $N_L$  leaks having coordinates  $z_n$ ,  $n = 1, \dots, N_L$ , and characteristic sizes  $\alpha_n$ ,  $n = 1, \dots, N_L$ , in which  $z_U < z_1 < \dots < z_{N_L} < z_m$ , and  $z_m$  denoting the measurement station site in a reservoir-pipe-valve system, as shown in Figure 1, is considered. The developed formulations are exploited to answer the questions raised earlier.

### 3. The Lower Bound Uncertainty Quantification of Multiple Leaks

The estimation model of the leak parameters comprises observations or measurements and the computational solver. Corresponding to this estimation model, the CRLB offers a lower bound limit on the covariance matrix of the unknown parameters that no unbiased estimator can exceed. After presenting the CRLB, which depends on computational state estimation, the approach to compute the pressure head states is elaborated in this section. The measurements, which are the sole source of uncertainty, are considered independent and identically distributed (i.i.d.) and Gaussian. The adopted state estimation model, which is assumed free of modeling error, evaluates the amplitudes corresponding to each frequency in viscoelastic (Keramat & Haghghi, 2014; Keramat et al., 2014) and elastic pipelines based on the transfer matrix solution of the water hammer equations.

#### 3.1. The Cramer-Rao Lower Bound Theory

Let the vector  $\theta$  denote the unknowns of the leak identification process with the following entries

$$\theta = (\mathbf{z}_L; \boldsymbol{\alpha}_L) = (z_1, z_2, \dots, z_N, \alpha_1, \alpha_2, \dots, \alpha_{N_L})^T \quad (1)$$

and  $\sigma^2$  be the noise variance. The lower bound uncertainty and correlation of the estimated parameters, that is,  $\text{cov}(\hat{\theta})$  can be found via (Casella, 2002)

$$\Sigma_{\hat{\theta}} = \Sigma(\hat{\theta}) \geq \frac{\sigma^2}{2} \left( \Re \left( \frac{\partial \mathbf{h}^H}{\partial \theta} \frac{\partial \mathbf{h}}{\partial \theta} \right) \right)^{-1} = \text{cov}(\hat{\theta}) \quad (2)$$

where  $\Re$  stands for the real part of a complex number (matrix), and variables with the circumflex represent an estimate of the unknown parameters. It is worthy throughout this study to distinguish between the covariance matrix (or variances) and the lower bound of the covariance matrix (or variances). To this end, the “variance” and “covariance” are denoted by  $\sigma^2, \Sigma$  and their lower bound are respectively indicated by “var” and “cov”. The inequality (Equation 2) is derived in the following based on the CRLB theory. In the leak detection problem, the leak properties are found by some measurement vectors  $\mathbf{h}^M$  whose elements are i.i.d and contaminated by white noise. The expected value (indicated by  $\mathbb{E}$ ) of the uncertain measurements are quantified by the transient model, hence

$$\mathbb{E}(\mathbf{h}^M) = \mathbf{h}, \quad (3)$$

and their covariance (denoted by  $\Sigma$ ) becomes

$$\Sigma_{\mathbf{h}^M} = \Sigma(\mathbf{h}^M) = \mathbb{E} \left[ (\mathbf{h}^M - \mathbf{h})(\mathbf{h}^M - \mathbf{h})^H \right], \quad (4)$$

which reduces to the noise variance ( $\sigma^2$ ) times the identity matrix on account of the i.i.d. assumption on the elements of  $\mathbf{h}^M$

$$\sigma^2(\mathbf{h}^M) = \sigma_{\mathbf{h}^M}^2 = \frac{1}{N_s \cdot J} \mathbb{E} \left[ (\mathbf{h}^M - \mathbf{h})(\mathbf{h}^M - \mathbf{h})^H \right] = \sigma^2, \Sigma(\mathbf{h}^M) = \sigma^2 \mathbf{I}_{N_s \cdot J} \quad (5)$$

where  $N_s, J$  are the number of measurement stations and transient data points at each station, and  $\mathbf{I}_{N_s \cdot J}$  is the identity matrix of size  $(N_s \cdot J)$  being the sample size. The log-likelihood of the identified leak characteristics then takes the following form (Wang & Ghidaoui, 2018)

$$\ln L(\theta; \mathbf{h}^M) = -\frac{(N_s \cdot J)}{2} \ln(2\pi) - (N_s \cdot J) \ln \sigma - \frac{1}{\sigma^2} \|\mathbf{h}^M - \mathbf{h}\|^2, \quad (6)$$

which enables to define of the Fisher information matrix  $\mathbf{F}_\theta$ . The CRLB theory provides the lower bound for the covariance matrix of the estimated leak unknowns via

$$\Sigma_{\hat{\theta}} = \Sigma(\hat{\theta}) = \mathbb{E} \left[ (\hat{\theta} - \theta)(\hat{\theta} - \theta)^T \right] \geq \mathbf{F}_\theta^{-1} \quad (7)$$

in which the elements of the Fisher information matrix are given by:

$$F_{p,q} = \mathbb{E} \left[ \frac{\partial \ln L(\theta; \mathbf{h}^M)}{\partial \theta_p} \frac{\partial \ln L(\theta; \mathbf{h}^M)}{\partial \theta_q} \right] = -\mathbb{E} \left[ \frac{\partial^2 \ln L(\theta; \mathbf{h}^M)}{\partial \theta_p \partial \theta_q} \right], p, q = 1, 2, \dots, 2N_L \quad (8)$$

One can refer to Appendix A of Kay (1993) for the derivation of the second equality. The expanded representation of the resulting matrix in Equation 8 is:

$$\mathbf{F}_\theta = -\mathbb{E} \partial^2 \ln L \begin{bmatrix} \frac{1}{\partial z_1^2} & \frac{1}{\partial z_1 \partial z_2} & \cdots & \frac{1}{\partial z_1 \partial z_{N_L}} & \frac{1}{\partial z_1 \partial \alpha_1} & \cdots & \frac{1}{\partial z_1 \partial \alpha_{N_L}} \\ \frac{1}{\partial z_2 \partial z_1} & \frac{1}{\partial z_2^2} & \cdots & \frac{1}{\partial z_2 \partial z_{N_L}} & \frac{1}{\partial z_2 \partial \alpha_1} & \cdots & \frac{1}{\partial z_2 \partial \alpha_{N_L}} \\ \vdots & & \ddots & & & & \vdots \\ \frac{1}{\partial z_{N_L} \partial z_1} & \frac{1}{\partial z_{N_L} \partial z_2} & \cdots & \frac{1}{\partial z_{N_L}^2} & \frac{1}{\partial z_{N_L} \partial \alpha_1} & \cdots & \frac{1}{\partial z_{N_L} \partial \alpha_{N_L}} \\ \frac{1}{\partial \alpha_1 \partial z_1} & \frac{1}{\partial \alpha_1 \partial z_2} & \cdots & \frac{1}{\partial \alpha_1^2} & \cdots & \frac{1}{\partial \alpha_1 \partial \alpha_{N_L}} & \\ \vdots & & & & \ddots & & \vdots \\ \frac{1}{\partial \alpha_{N_L} \partial z_1} & \frac{1}{\partial \alpha_{N_L} \partial z_2} & & \cdots & & & \frac{1}{\partial \alpha_{N_L}^2} \end{bmatrix} \quad (9)$$

Appendix A illustrates details to compute the derivatives of the likelihood function, that is, the elements of the Fisher information matrix in Equation 9 which are evaluated based on the modeled transient pressures.

The simplifications in Appendix A allow for the following plain representation of the elements of the Fisher information matrix

$$\mathbf{F}_\theta = \frac{2}{\sigma^2} \begin{bmatrix} \left\| \frac{\partial \mathbf{h}}{\partial z_1} \right\|^2 & \Re \left( \frac{\partial \mathbf{h}^H}{\partial z_1} \frac{\partial \mathbf{h}}{\partial z_2} \right) & \dots & \Re \left( \frac{\partial \mathbf{h}^H}{\partial z_1} \frac{\partial \mathbf{h}}{\partial \alpha_1} \right) & \Re \left( \frac{\partial \mathbf{h}^H}{\partial z_1} \frac{\partial \mathbf{h}}{\partial \alpha_2} \right) & \dots & \Re \left( \frac{\partial \mathbf{h}^H}{\partial z_1} \frac{\partial \mathbf{h}}{\partial \alpha_{N_L}} \right) \\ \Re \left( \frac{\partial \mathbf{h}^H}{\partial z_2} \frac{\partial \mathbf{h}}{\partial z_1} \right) & \left\| \frac{\partial \mathbf{h}}{\partial z_2} \right\|^2 & \dots & \Re \left( \frac{\partial \mathbf{h}^H}{\partial z_2} \frac{\partial \mathbf{h}}{\partial \alpha_1} \right) & \Re \left( \frac{\partial \mathbf{h}^H}{\partial z_2} \frac{\partial \mathbf{h}}{\partial \alpha_2} \right) & \dots & \Re \left( \frac{\partial \mathbf{h}^H}{\partial z_2} \frac{\partial \mathbf{h}}{\partial \alpha_{N_L}} \right) \\ \vdots & \vdots & \ddots & \vdots & \vdots & \vdots & \vdots \\ \Re \left( \frac{\partial \mathbf{h}^H}{\partial z_{N_L}} \frac{\partial \mathbf{h}}{\partial z_1} \right) & \Re \left( \frac{\partial \mathbf{h}^H}{\partial z_{N_L}} \frac{\partial \mathbf{h}}{\partial z_2} \right) & \dots & \left\| \frac{\partial \mathbf{h}}{\partial z_{N_L}} \right\|^2 & \Re \left( \frac{\partial \mathbf{h}^H}{\partial z_{N_L}} \frac{\partial \mathbf{h}}{\partial \alpha_1} \right) & \dots & \Re \left( \frac{\partial \mathbf{h}^H}{\partial z_{N_L}} \frac{\partial \mathbf{h}}{\partial \alpha_{N_L}} \right) \\ \Re \left( \frac{\partial \mathbf{h}^H}{\partial \alpha_1} \frac{\partial \mathbf{h}}{\partial z_1} \right) & \Re \left( \frac{\partial \mathbf{h}^H}{\partial \alpha_1} \frac{\partial \mathbf{h}}{\partial z_2} \right) & \dots & \dots & \left\| \frac{\partial \mathbf{h}}{\partial \alpha_1} \right\|^2 & \dots & \Re \left( \frac{\partial \mathbf{h}^H}{\partial \alpha_1} \frac{\partial \mathbf{h}}{\partial \alpha_{N_L}} \right) \\ \vdots & \vdots & \vdots & \vdots & \vdots & \vdots & \vdots \\ \Re \left( \frac{\partial \mathbf{h}^H}{\partial \alpha_{N_L}} \frac{\partial \mathbf{h}}{\partial z_1} \right) & \Re \left( \frac{\partial \mathbf{h}^H}{\partial \alpha_{N_L}} \frac{\partial \mathbf{h}}{\partial z_2} \right) & \dots & \dots & \dots & \dots & \left\| \frac{\partial \mathbf{h}}{\partial \alpha_{N_L}} \right\|^2 \end{bmatrix} \quad (10)$$

$$= \frac{2}{\sigma^2} \Re \left( \frac{\partial \mathbf{h}^H}{\partial \theta} \frac{\partial \mathbf{h}}{\partial \theta} \right)$$

in which  $\Re$  stands for the real part of the evaluated number given the real nature of the leak size and location error. Considering Equations 1, 7, and 10 the lower bounds of the leak unknowns are achieved as presented in Equation 2. Appendix B offers another approach to derive inequality (Equation 2) based on the Taylor series.

The inequality (Equation 2) is general and applicable to any pipe system as long as a proper transient model for that system to compute the pressures is available. In the next section, the water hammer model for a reservoir-pipe-valve system with multiple leaks is elaborated.

### 3.2. The State Estimation Model

This section presents the formulation to compute the pressure and head spectra along the pipeline for a reservoir-pipe-valve system, which enables computing the terms of the CRLB expressions.

Let  $\alpha_n$ ,  $n = 1, \dots, N_L$  denote the characteristic size of each leak which is determined by steady-state leakage flow rate  $Q_{Ln}^0$ , its pressure head  $H_{Ln}^0$  and elevation  $y_{Ln}$ . In view of the linearized (in terms of the leak sizes  $\alpha_n$ ,  $n = 1, 2, \dots, N_L$ ) form of the transient response, the elements of the pressure head (corresponding to each frequency) at the  $m$ th measurement station are computed as:

$$h_m = \left( m_{21}^{N_L} + \sum_{n=1}^{N_L} \alpha_n m_{21}^{S_{Ln}^m} \right) q_U = \frac{m_{21}^{N_L m} + \sum_{n=1}^{N_L} \alpha_n m_{21}^{S_{Ln}^m}}{m_{11}^{N_L D} + \sum_{n=1}^{N_L} \alpha_n m_{11}^{S_{Ln}^D}}, \quad (11)$$

$$m_{11}^{N_L D} = \cosh(\mu z_d),$$

$$m_{11}^{S_{Ln}^D} = -\vartheta \cosh(\mu z_{nm}) \sinh(\mu z_{Un}), \quad m_{21}^{N_L m} = -\vartheta \sinh(\mu z_d),$$

$$m_{22}^{N_L m} = \cosh(\mu z_d), \quad m_{21}^{S_{Ln}^m} = \vartheta^2 \sinh(\mu z_{nm}) \sinh(\mu z_{Un}),$$

$$m_{22}^{S_{Ln}^m} = -\vartheta \cosh(\mu z_{Un}) \sinh(\mu z_{nm}), \quad z_d = z_m - z_U,$$

$$z_{nm} = z_m - z_n, \quad z_{Un} = z_n - z_U, \quad \alpha_n = -\frac{Q_{Ln}^0}{2(H_{Ln}^0 - y_{Ln})},$$

$$m = 1, 2, \dots, N_s, \quad n = 1, 2, \dots, N_L$$

where,  $z_m$ ,  $m = 1, 2, \dots, N_s$  represent the location of the measurement station,  $z_U$  stands for the coordinate of the upstream node, and  $\vartheta$  and  $\mu$  are respectively the characteristic impedance and the propagation function as follows

**Table 1**  
The Pipe and Flow Specifications of the Numerical Case Study

Length	$L = 2,000$ m
Inner diameter of the pipe wall	$D = 0.5$ m
Elastic modulus of the pipe wall	$E = 210$ GPa
Thickness of the pipe wall	$e = 1$ cm
Bulk modulus of the fluid	$K = 2.1$ GPa
Upstream reservoir head	$h_R = 25$ m
Outflow rate from the reservoir	$Q^0 = 15.3$ Ls <sup>-1</sup>
Leakage flow rate	$Q_L^0 = 3$ Ls <sup>-1</sup>
Effective leak size	$A_e = 140$ mm <sup>2</sup>
Fluid's density	$\rho_f = 1,000$ kg m <sup>-3</sup>
Friction factor	$f = 0.02$
Wave speed	$a_E = 1,200$ ms <sup>-1</sup>

$$\vartheta = \frac{\mu a^2}{i\omega Ag}, \quad \mu = \frac{i\omega}{a} \sqrt{1 + \frac{f q_0}{i\omega AD}}, \quad i = \sqrt{-1} \quad (12)$$

in which the Darcy-Weisbach friction factor  $f$ , gravitational acceleration  $g$ , inner diameter of pipe  $D$ , cross-sectional area of flow  $A$ , steady-state flow rate  $q_0$ , and wave speed  $a$  are independent input parameters, and  $\omega$  represents the frequencies. In the case of the viscoelastic pipe, the frequency-dependent wave speed as defined by Karimian et al. (2020) is used. Equation 11 is derived on account of the transfer matrix approach once used to compute the heads and flow rates at the measurement stations (Chaudhry, 2014).

#### 4. Numerical Case Study, Verification, and Discussion

This section seeks to investigate the theoretical formulations derived earlier through numerical examples. Considering the main target of this paper to estimate the error bound of the leak detection and noting that such an error depends on the estimation model, this section is organized as follows. First, the specifications of the pipe system to analyze the uncertainty quantification of leaks parameters are provided. Second, the Monte Carlo simulations (Hastings, 1970) of the leakage estimator proposed by Keramat and

Duan (2021) and the maximum reflections theories developed by Louati et al. (2020) are employed to validate the formulae in inequality (Equation 2) for the covariance matrix of leaks.

##### 4.1. Preliminaries

The typical reservoir-pipe-valve system with a few leaks, as depicted in Figure 1, with specifications in Table 1, is considered for the localization and error estimation. The location of the measurement station is set to  $z_D = 2,000$  m (the downstream boundary) whose data are indicated by the superscript  $M$  in the derived formulations. The collected transient pressure data are assumed to follow the normal distribution. To this end, the noise-free data are first evaluated using the transient model and then both their real and imaginary parts are separately added to zero-mean Gaussian random vectors to produce the noisy measurements hypothetically.

##### 4.2. The Standard Monte Carlo Sampling

The formula derived in inequality (Equation 2) and the resulting expression for  $\mathbf{h}$  can be used to find the lower bound of the covariance matrix of the estimated parameters. For the case of a single leak with  $z_L, \alpha_L$  parameters, Equation 10 reduces to

$$\text{cov}(\hat{z}_L, \hat{\alpha}_L) = \sigma^2 \left[ \begin{array}{cc} \left\| \frac{\partial \mathbf{h}}{\partial z_L} \right\|^2 & \Re \left( \frac{\partial \mathbf{h}^H}{\partial z_L} \frac{\partial \mathbf{h}}{\partial \alpha_L} \right) \\ \Re \left( \frac{\partial \mathbf{h}^H}{\partial \alpha_L} \frac{\partial \mathbf{h}}{\partial z_L} \right) & \left\| \frac{\partial \mathbf{h}}{\partial \alpha_L} \right\|^2 \end{array} \right]^{-1} \leq \begin{bmatrix} \sigma^2(\hat{z}_L) & \Sigma(\hat{z}_L, \hat{\alpha}_L) \\ \Sigma(\hat{z}_L, \hat{\alpha}_L) & \sigma^2(\hat{\alpha}_L) \end{bmatrix} \quad (13)$$

in which the diagonal elements are variances of the leak location and size estimate and the off-diagonal elements correspond to the covariances. A detailed definition of each entry of the Fisher Information matrix (at the left-hand side of the inequality) can be found in Appendix C.

The main focus of this section is to verify the derived relations for the uncertainty of estimated parameters, among which the lower bound of the standard deviation of the leak location estimates corresponds to the square root of the first entry of the matrix depicted on the left-hand side of the inequality (Equation 2). Being of particular importance in real practice, Figure 2 plots this quantity for various locations of the actual leak in black dashed line, in which (a) corresponds to the case that only five resonant frequencies are used in localization and (b) is obtained for  $\omega_{\max} = 7\omega_{th}$  as the bandwidth of used frequencies.

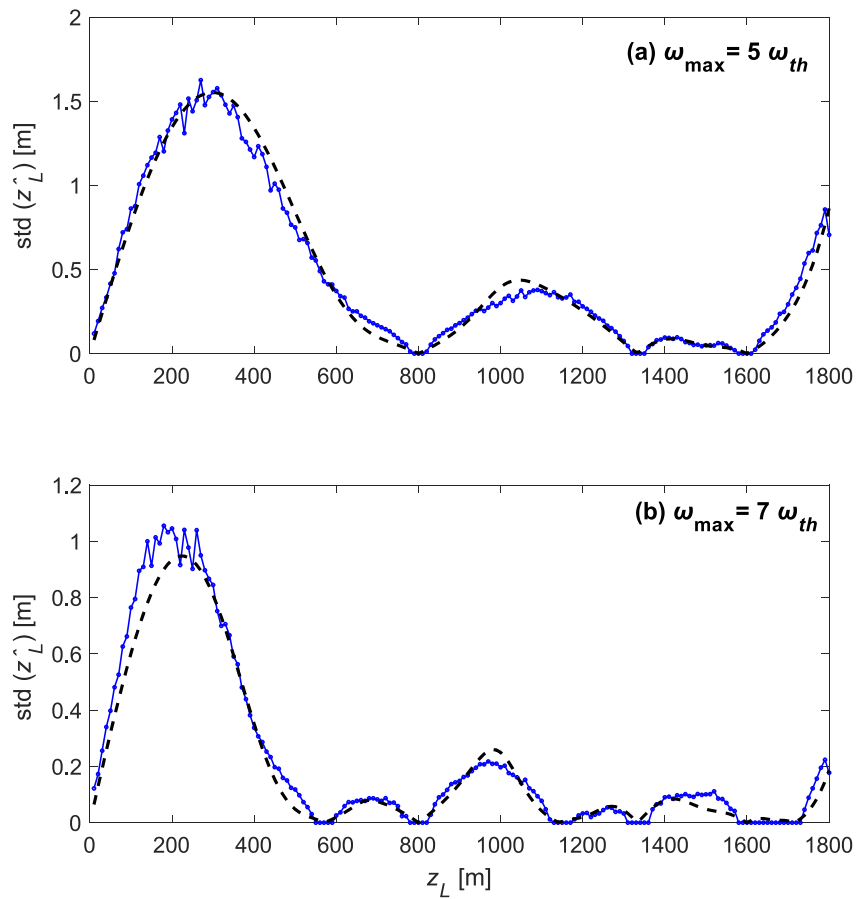


**Figure 2.** The standard deviation of the leak location estimates for various leak positions along the pipeline. The standard deviation results are obtained through exhaustive Monte Carlo trials (the continuous blue curve) and the proposed formula (the dashed black curve).

To examine Figure 2, the estimator recently proposed by Keramat and Duan (2021) is used to find the error of the identified leak locations once the leak is placed at different points along the pipeline. However, because of the sensitivity of the estimation results to the transient signal, which is noisy and uncertain, the feasible approach is to find different realizations of the transient data. Using the different sets of collected data, the leak location is separately estimated so as to infer the desired parameters of the distribution corresponding to the leak location. Established as the exhaustive Monte Carlo approach, the results of each individual localization  $\hat{z}_{Lr}$ ,  $r = 1, 2, \dots, N_{MC}$ , in which  $N_{MC}$  is the total number of the localizations, can then be used to arrive at the standard deviation of the leak location or  $\text{std}(\hat{z}_L)$ ,

$$\text{std}(\hat{z}_L) = \sqrt{\frac{\sum_{r=1}^{N_{MC}} (\hat{z}_{Lr} - z_L)^2}{N_{MC}}} \quad (14)$$

Note that the higher the  $N_{MC}$ , the closer the results get to the standard deviation or to the lower bound defined in this research. In the numerical case of this study,  $N_{MC} = 300$  could provide satisfactory results. Now, the illustrated approach can be employed for different value of  $z_L$  to infer the significance of the actual location of the leak in the localization accuracy. The blue circles in Figure 2a indicate the  $\text{std}(\hat{z}_L)$  for  $z_L = \{10 : 10 : 1,800\}$ , which as seen, that is of larger quantity at 300 m than 600 m, or  $\text{std}(z_L = 300 \text{ m}, \hat{z}_L) > \text{std}(z_L = 600 \text{ m}, \hat{z}_L)$ . This finding is consistent with the fact that various locations of the actual leaks are subject to identifications of a different order of accuracy.

As shown in Figure 2, the proposed formula and the Monte Carlo depicted respectively in dashed black line and the continuous blue favorably match each other. The comparison is satisfactory given the fact that first, theoretically,

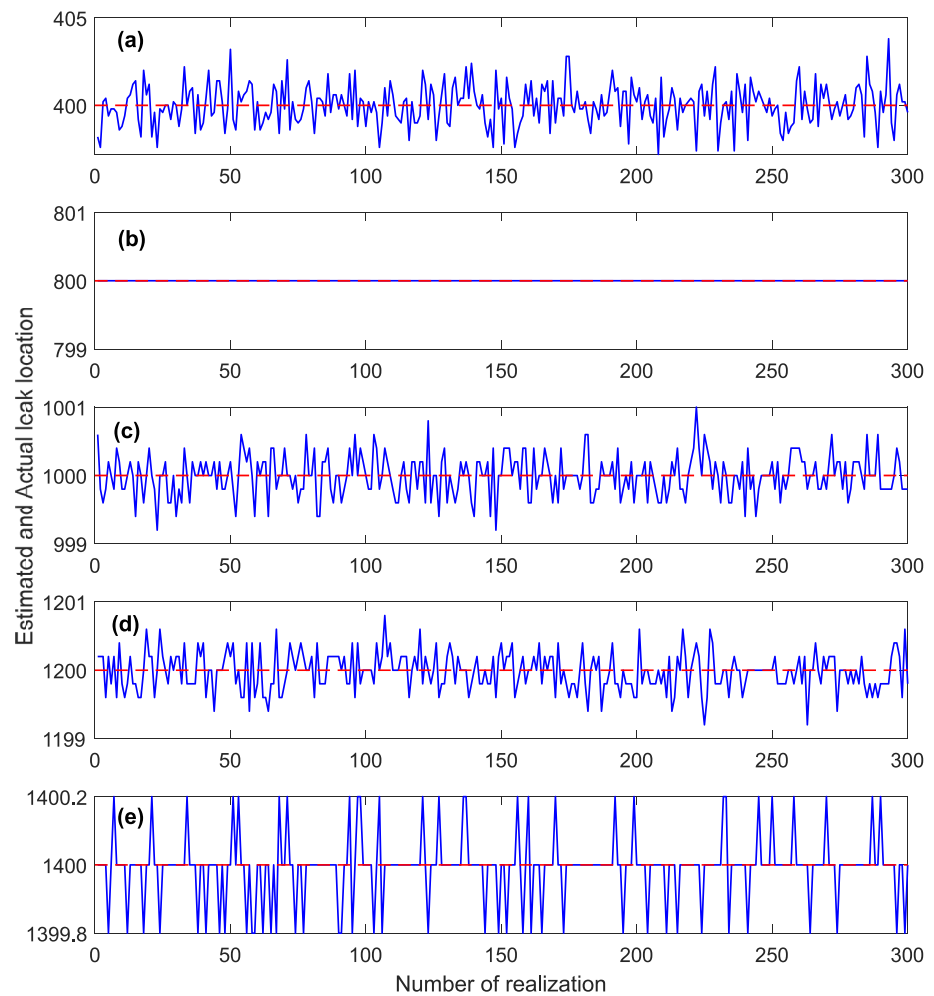


**Figure 3.** Manifestation of the leak detection results (the blue lines) for several Monte Carlo realizations ( $N_{MC} = 300$ ) at various locations of the actual leak (the dashed red lines); (a)  $z_L = 400$  m, (b)  $z_L = 800$  m, (c)  $z_L = 1,000$  m, (d)  $z_L = 1,200$  m, (e)  $z_L = 1,400$  m.

the number of stimulations,  $N_{MC}$  should approach infinity to get the correct value. Second, this is, in fact, a check for many points along the pipeline (each of which requires 300 simulations to find the indicated value, i.e., each blue circle is the result of Equation 14 for a specific  $z_L$ ). Figure 3 displays the results of each of these localizations for various positions of the actual leak (the dashed red lines) (a)  $z_L = 400$  m, (b)  $z_L = 800$  m, (c)  $z_L = 1,000$  m, (d)  $z_L = 1,200$  m, (e)  $z_L = 1,400$  m. The result in Figure 2 reveals that the incorporated estimator (Keramat & Duan, 2021) achieves the CRLB so that it can be called fully efficient in the sense that it makes full use of the transient data (Casella, 2002). It will be instructive to recall the difference between the estimator and the estimation model. The estimator refers to a method employed to arrive at an estimate of the desired parameter. But the estimation model is associated with a particular set of information (data) and mathematical/computational model. Each estimation model has a unique CRLB. For one estimation model, several estimators may exist, among which the one whose variance achieves the CRLB (as shown in Figure 2) is called fully efficient.

It is worthwhile to note that the uncertainties depicted in Figure 2 are proportional to the noise standard deviation as seen in inequality (Equation 2). The reason for choosing a small standard deviation  $\sigma$  which has led to small localization errors in Figure 2, is that the required number of Monte Carlo simulations will be huge for higher noise levels, thus complicating the verification. Nevertheless, the results in this figure indicate that the error at some locations is far more than some other locations, which suggests the necessity of providing these results along with the localization results to give the clients a level of reliability to the reports. A related strange issue in

these results is the significant drop of localization uncertainty around the upstream which will be explained later in terms of leak size uncertainty.

### 4.3. In-Depth Examination of the Identification Process and Uncertainty Quantification

The results obtained in Figure 2, especially the locations of tiny error, can be scrutinized via Equation 11 once it is written for a single leak if assuming a single measurement station at the valve  $z_m = L$ :

$$h_D = \frac{m_{21}^{NLm} + \alpha_L m_{21}^{SLm}}{m_{11}^{NLD} + \alpha_L m_{11}^{SLD}} = \frac{-\vartheta \sinh(\mu L) + \alpha_L \vartheta^2 \sinh(\mu(L - z_L)) \sinh(\mu z_L)}{\cosh(\mu L) - \alpha_L \vartheta \cosh(\mu(L - z_L)) \sinh(\mu z_L)} \quad (15)$$

$$= \frac{\vartheta i \sin(i\mu L) - \alpha_L \vartheta^2 \sin(i\mu(L - z_L)) \sin(i\mu z_L)}{\cos(i\mu L) + i \alpha_L \vartheta \cos(i\mu(L - z_L)) \sin(i\mu z_L)},$$

Noting that for a frictionless case,  $\mu = \frac{i\omega}{a} = i\kappa$ , Equation 15 reduces to:

$$h_D = \frac{-\vartheta i \sin(\kappa L) - \alpha_L \vartheta^2 \sin(\kappa(L - z_L)) \sin(\kappa z_L)}{\cos(\kappa L) - i \alpha_L \vartheta \cos(\kappa(L - z_L)) \sin(\kappa z_L)} \quad (16)$$

It is now instructive to revisit the leak detection procedure to decipher the reason behind the formation of the points of infinitesimal error in Figure 2. Basically, the localization of a single leak is based on fitting the leak parameters in Equation 16 (i.e.,  $\alpha_L$  and  $z_L$ ) such that the computed pressures based on this equation become as close as possible to the measured data. Consequently, in the case of a single leak, the pressure response corresponding to a few waves (i.e., the first few harmonics) will be enough to pinpoint the leak. Equation 16 implies that corresponding to each wave, there are points along the pipe at which their amplitude at the valve is maximum. These locations are in fact more sensitive to the pressure head formed at the valve node and therefore, the existence of a leak at these points can easily be identified by that specific wave. To further clarify the properties of these points, Equation 16 is plotted for various locations of the leaks  $0 < z_L < L$  throughout the pipe for each harmonic (second to fifth harmonic) as seen in Figures 4a–4d. One can now recognize that the minimum-error locations in Figure 2a that is  $z_L^* \in \{800, 1,333, 1,600\}$  m, and those in Figure 2b which are  $z_L^* \in \{571, 800, 1,143, 1,333, 1,600, 1,714\}$  m correspond to the extrema in Figures 4a–4d.

It is quite obvious that noise can hardly ruin the distinct amplitudes which correspond to the locations of minimum error. This is made observable in Figures 5a–5g which depicts an imposed uncertainty along with the pressure amplitude at the valve for the second harmonic  $\omega = 3\omega_{th}$ . Figure 5a is identical to Figure 4a and so is Figure 5b but with a refined vertical scale (notice the  $z_L^* = 1,333$  m as derived and discussed earlier). More refined shapes corresponding to different zones of potential leak locations: (c)  $200 \text{ m} < z_L < 250 \text{ m}$ , (d)  $400 \text{ m} < z_L < 450 \text{ m}$ , (e)  $1,100 \text{ m} < z_L < 1,150 \text{ m}$ , (f)  $1,700 \text{ m} < z_L < 1,750 \text{ m}$ , are also plotted. In all the figures (c–f) the error bars (in red) indicate *the same* noise standard deviation ( $\sigma = 1,000$  m), therefore the level of uncertainty that each of which brings about in the localization process can be appreciated. Figures 5d and 5f are subjected to higher uncertainty, and Figures 5c and 5e are prone to more accuracy as can also be verified through the CRLB curve explained earlier and also redrawn in Figure 5g. It is worthwhile to note that the representations in Figures 5a–5f are just for a single wave (the second harmonic) and hence cannot be considered as a solid basis for the accuracy of localization in general. Nevertheless, the curve in Figure 5g which combines the first and second resonant data provides the reliable tool to assess the best possible localization accuracy using the specified bandwidth.

As a further investigation for each specific wave, one can find the locus of minimum error by setting the denominator of Equation 16 to zero. The roots of the first term in the denominator provide the system resonant frequencies

$$\cos(\kappa L) = 0 \Rightarrow \kappa L = (2m - 1) \frac{\pi}{2} \Rightarrow \omega_m = (2m - 1) \frac{\pi a}{2L}, \quad m \in \mathbb{Z}^+ \quad (17)$$

in which  $\mathbb{Z}^+$  represents the set of positive integer numbers. The roots of the second term indicate specific locations at which the produced amplitude of that wave at the valve is maximum:

$$\sin(\kappa z_L) = 0 \Rightarrow \kappa z_L = n\pi \Rightarrow \omega_n = \frac{n\pi a}{z_L}, \quad n \in \mathbb{Z}^+ \quad (18)$$

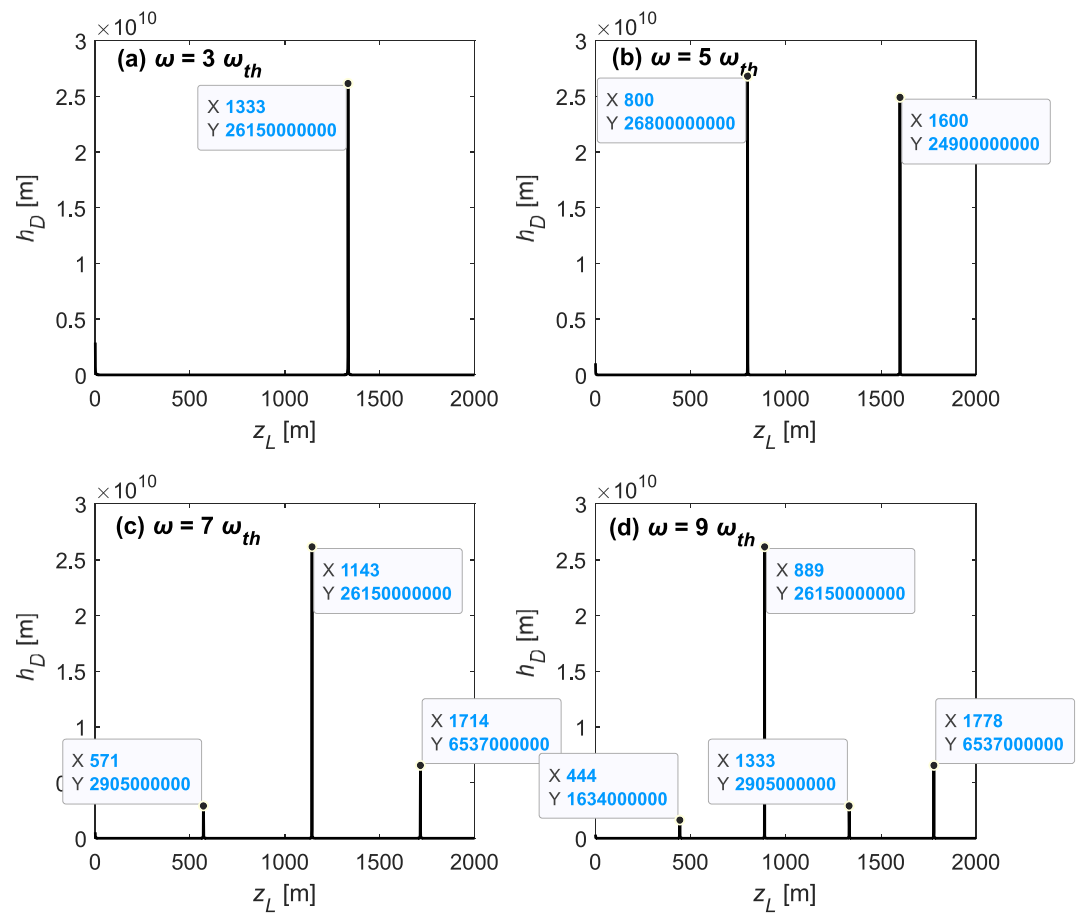


**Figure 4.** The amplitude of different waves; (a–d) respectively correspond to second, third, fourth and fifth harmonic wave at the valve versus all possible locations of the leak. The data tips indicate the locations of maximum amplitude corresponding to each specific wave.

The resonant waves given by Equation 17 and the frequencies corresponding to the locus of maximum amplitudes for each harmonic wave determined via Equation 18, can be equated to find the points of minimum error in the localization process, noting that  $0 < z_L^*/L < 1$ :

$$\omega_n = \omega_n \Rightarrow \frac{z_L^*}{L} = \frac{2n}{2m-1}, \quad 0 < \frac{z_L^*}{L} < 1 \Rightarrow 0 < n < m - \frac{1}{2}, \quad m, n \in \mathbb{Z}^+ \quad (19)$$

That means for the first wave, no such location of infinitesimal error exists or  $m = 1, n = \{\}$ ,  $z_L^* = \{\}$ , and likewise, for  $m = 2, n = \{1\}$ ,  $\frac{z_L^*}{L} = \left\{\frac{2}{3}\right\}$ , for  $m = 3, n = \{1, 2\}$ ,  $\frac{z_L^*}{L} = \left\{\frac{2}{5}, \frac{4}{5}\right\}$ , for  $m = 4, n = \{1, 2, 3\}$ ,  $\frac{z_L^*}{L} = \left\{\frac{2}{7}, \frac{4}{7}, \frac{6}{7}\right\}$ , and so on. Figure 6 lists the locations for  $m = 2, \dots, 9$  in the case of  $L = 2,000$  m, as shown in the data tips in the figure. Figures 7a–7d depicts the CRLB results corresponding to different range of frequencies that is  $\omega = \{(2m-1)\omega_{th} : m = 2, 3, 4, 5\}$ , along with the  $z_L^*$  quantities as data tips. There is again good agreement between the points of minimum error in Figure 7 and those predicted in Figure 6, noting that the space in Figure 7 was  $z_L = 10 : 10 : 2,000$  m.

## 5. Application to Leakage Identification

The quantified uncertainties corresponding to the estimated parameters can provide useful information for enhanced localization, as evidenced in various research areas. For example, in structural damage detection, G. Wang (2018), and in structural health monitoring, Yue and Aliabadi (2020) offered improved techniques by utilizing the evaluated uncertainties. In this section, the uncertainty formulations drawn in the previous section

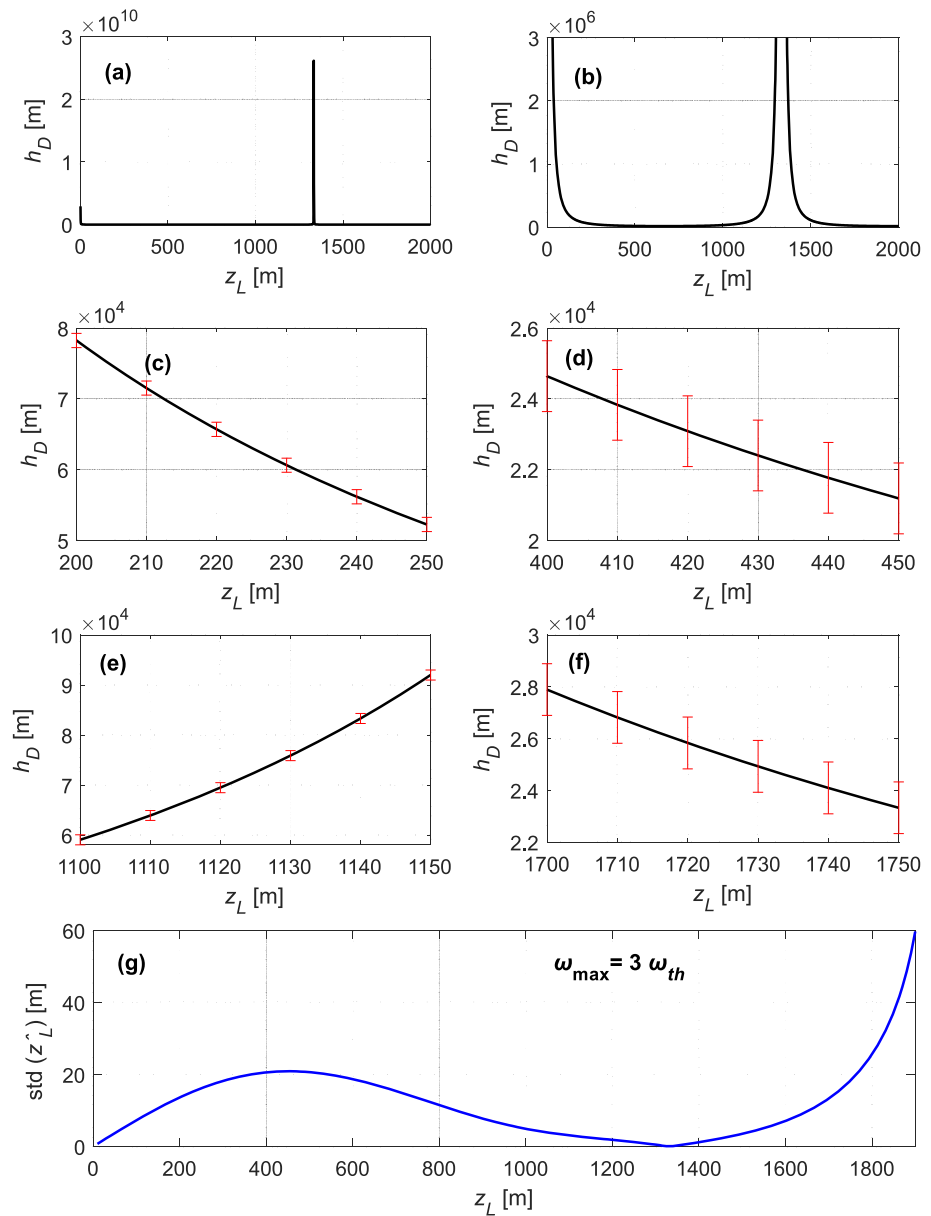


**Figure 5.** (a) The computed  $h_D$  at the valve for the second harmonic versus all possible leak locations; (b) a refined (in vertical scale) representation of (a); (c–f) further resolution of (a) for specific zone along the pipe as indicated in the horizontal axis; (g) standard deviation of the localization estimates for various leak positions along the pipeline.

will be exploited for efficient leak detection. The efficiency refers to using an appropriate number of resonant frequencies and corresponding amplitudes, which is essential for leak identification exercises in actual practice.

### 5.1. Localization Error Variations With the Signal Bandwidth

The estimate of the minimum error depends on the actual leak location, the employed frequencies ( $\omega_{\max}$ ,  $\Delta\omega$ ), and the noise variance ( $\sigma^2$ ). The computed errors in the case of a single leak are shown in Figure 8, which depicts the variation of the lower bound of the localization error (vertical axis) versus location and signal bandwidth (the maximum number of modes used in the identification, i.e.,  $m_{\max} = \omega_{\max}/\omega_{th}$ ; Lee et al., 2015). In other words, it indicates how different leaks placed at  $z_L \in \{50 : 50 : 1,800\}$  require a different number of resonant peaks

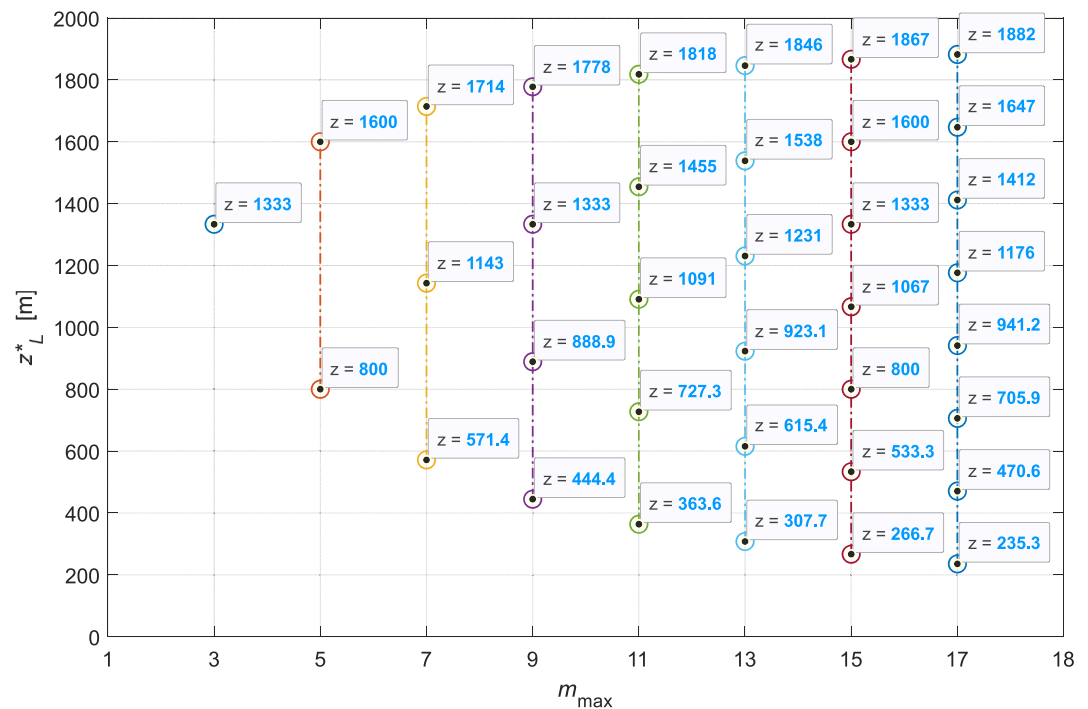


**Figure 6.** The locations of infinitesimal error corresponding to each wave  $m = 2, \dots, 9$  (the horizontal axis) for  $L = 2,000$  m.

to provide the same localization accuracy. The reason for the step-like variations is that even harmonics give no information, and hence, only the odd harmonics enhance the localization (when using the valve signal). It is also worth noting that for all leak locations, the use of more frequencies contributes to less uncertainty, or in other words, the displayed error curves are monotonically decreasing.

The preceding figure offers information about the estimation error for a given leak set after the leak identification. To use this kind of results in the actual practice of leak detection, one may consider the identified location as the actual one and then estimate the error using the approach provided in this research, that is, inequality (Equation 2). With this, the error graphs offer meaningful information about the reliability and preciseness of the solution outcome (Diong et al., 2015), which will be discussed in the next section. The formulations in (Equation 2) are general and applicable to the multiple-leak case. In practice, one can report the identified leak results and the corresponding error (minimum possible standard deviation) to provide the clients with further insight into potential uncertainty arising from noise on collected data (Lambert, 2012). Note that the Bayesian modeling suggested by Alawadhi and Tartakovsky (2020) is another approach to provide the probability of the successful localization, and apply it in the localization process, but the proposed approach in this research is extremely simpler as it provides analytical formulations and does not require any sampling, integration or solving differential equations.

### 5.2. A Noise-Efficient Algorithm for Leak Detection

This section seeks to apply the foregoing research achievements to decide how many resonant frequencies are appropriate for the localization. In the case of noise-free signals, Gong et al. (2013) and later Du et al. (2020, 2021) found that the first three resonant frequencies are enough to pinpoint a leak. But, when noise is administrated as an influential aspect in the localization, as revealed by the CRLB theory, the leak's position will be a fundamental parameter determining the accuracy of the leak location identification. To this end, a single leak detection problem with a relatively high noise level is scrutinized when localization with different bandwidths ( $m_{\max}$ ) is considered.

The leak size and location are  $A_e = 140 \text{ mm}^2$  and  $z_L = 860 \text{ m}$  respectively. By a close look at Figure 6, the nearest minimum error points ( $z^*$ ) to this leak location ( $z_L = 860 \text{ m}$ ) for  $3 \leq m_{\max} \leq 15$  are  $\{800.0, 888.9, 727.3, 923.1\} \text{ m}$

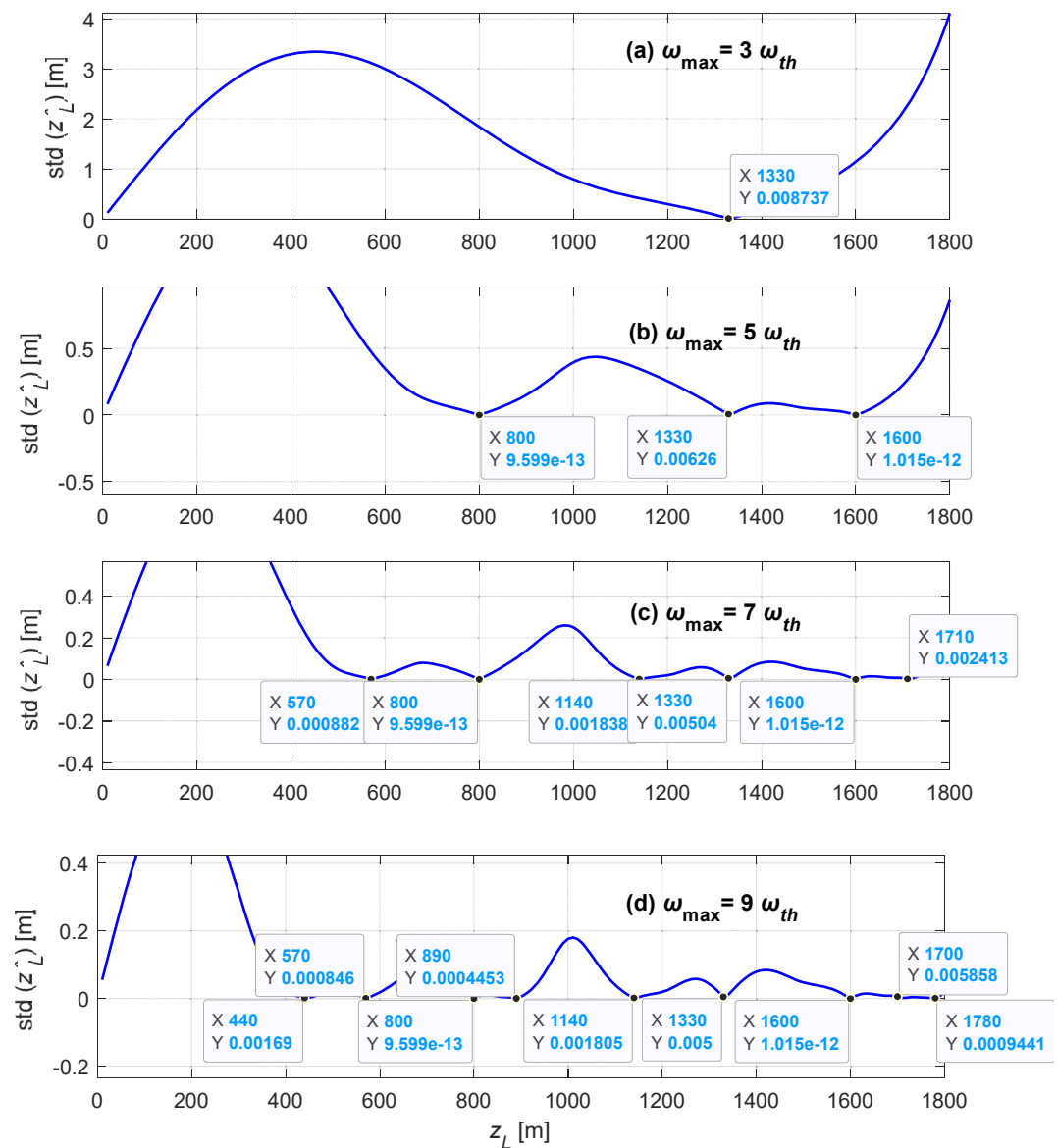


**Figure 7.** The minimum standard deviations versus various leak positions along the pipeline for different range of used frequencies (a)  $\omega_{\max} = 3\omega_{th}$ , (b)  $\omega_{\max} = 5\omega_{th}$ , (c)  $\omega_{\max} = 7\omega_{th}$ , (d)  $\omega_{\max} = 9\omega_{th}$ . The data tips indicate where the error is extremely small.

which respectively correspond to  $\frac{z_L^*}{L} = \left\{ \frac{2}{5}, \frac{4}{9}, \frac{4}{11}, \frac{6}{13} \right\}$ , and  $m_{\max} = 5, 9, 11, 13$ . The differences of these points from the actual leak location are  $|z_L^* - z_L| = \{60.0, 28.9, 132.7, 63.1\}$  m, so that the nearest point is  $\frac{z_L^*}{L} = \left\{ \frac{4}{9} \right\}$ , thus expecting that  $m_{\max} = 9$  is the best bandwidth to use for localization, as will be demonstrated in the following.

To see the effect of the noise structure in actual practice, we generate noisy transient data (SNR 20 dB) and use them for localization with several signal bandwidths as shown in Figure 9. As seen, in all cases, the signal of bandwidth  $m_{\max} = 9$  performs quite satisfactorily. But, more importantly, higher frequencies ( $m_{\max} > 9$ ) start to produce unstable localizations depending on the noise level. The figure only shows a few results to better address the issue after running the localization process and investigating the pattern of all consequences several times.

One may presume that using more resonant frequencies always leads to enhance accuracy. However, two findings contradict this conjecture: (a) as discovered in this study, leaks placed at different locations require different

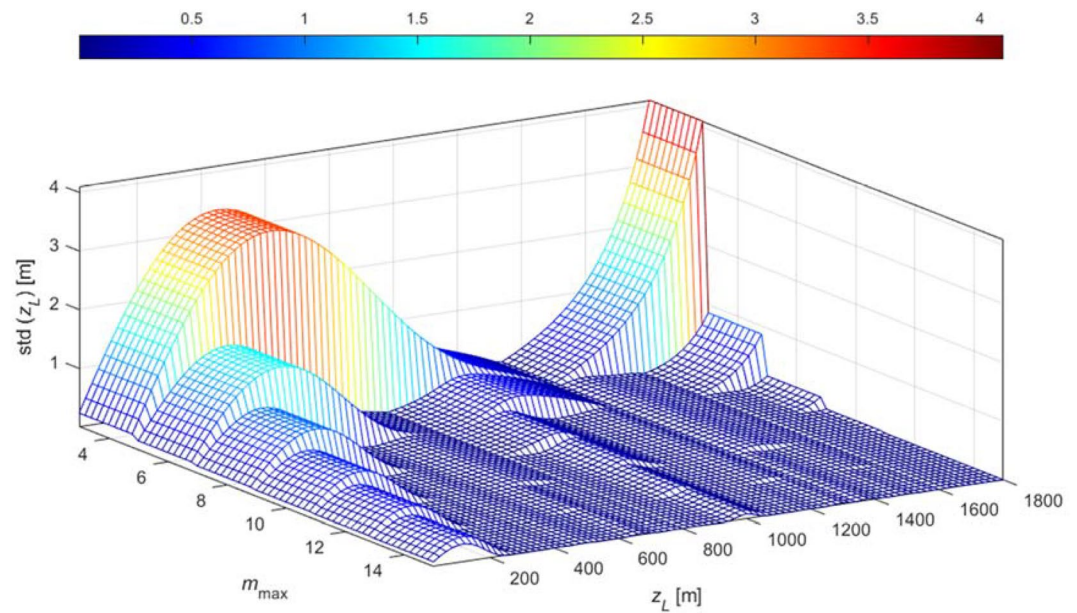


**Figure 8.** The variation of the lower bound of localization error corresponding to each employed signal bandwidth versus different location candidates along the pipe ( $m_{\max} = \omega_{\max}/\omega_{th}$ ).

resonant peaks to arrive at the same accuracy. For example, some cases only need the first and third resonant amplitudes to pinpoint the leak location (i.e., those at or very close to  $z_L^* = 1,333$  m), and using more has no effects on the accuracy; (b) high resonant frequencies are less reliable since they are subject to more significant contamination with noise, which has a high-frequency structure. Accordingly, the best advice is to use the minimum possible number of resonant peaks for the identification. In other words, the workflow depicted in Figure 10 can be employed for leak detection, thus allowing for an efficient application of the collected transient data. The following points worth noting regarding this flowchart:

1. The bandwidth of the collected signal denoted by  $m_{BW}$  is different than the bandwidth incorporated in the identification process.  $m_{BW}$  is decided by inspecting the signal only, as will be seen in the subsequent experimental studies.
2. The estimated errors in inequality (Equation 2) are minimum possible uncertainty which may be far from what we get by a single set of data in reality. In fact, by definition, it corresponds to the standard deviation of the localization distribution, which is found when many localizations are carried out. However, it is achievable in actual practice, that is, repeat the localization several times corresponding to several measured data sets. Alternatively, several measurements (with the same characteristics, that is, measurement location, structural and hydraulic state of the pipe system, etc.) may be averaged to find the mean signal to be exploited for leak detection. Under this circumstance, the estimated error, which is supposed to be relatively low, is a reliable approximate to those given by inequality (Equation 2).
3. In this flowchart and all simulations carried out in this section, the frequency step is set to  $\Delta\omega = 2\omega_{th}$  so that only resonant frequencies (odd harmonics) are used. The reason is that the pipe system is less sensitive to other frequencies, especially the even harmonics for which the corresponding amplitudes at the valve are nil. Consequently, more noise is absorbed using amplitudes different than resonant frequencies, while in return, no significant information is incorporated in the solution process.

## 6. Experimental Case Studies and Discussion

In this section, two experimental case studies are investigated with the aim of further clarifying the significance of the proposed formulations. The first experiment studies the single leak case in which the uncertainties are reported when different signal bandwidths are used for localization. The second experiment investigates the double leaks problem and the associated uncertainties when noisy measurements are used to pinpoint the leaks.

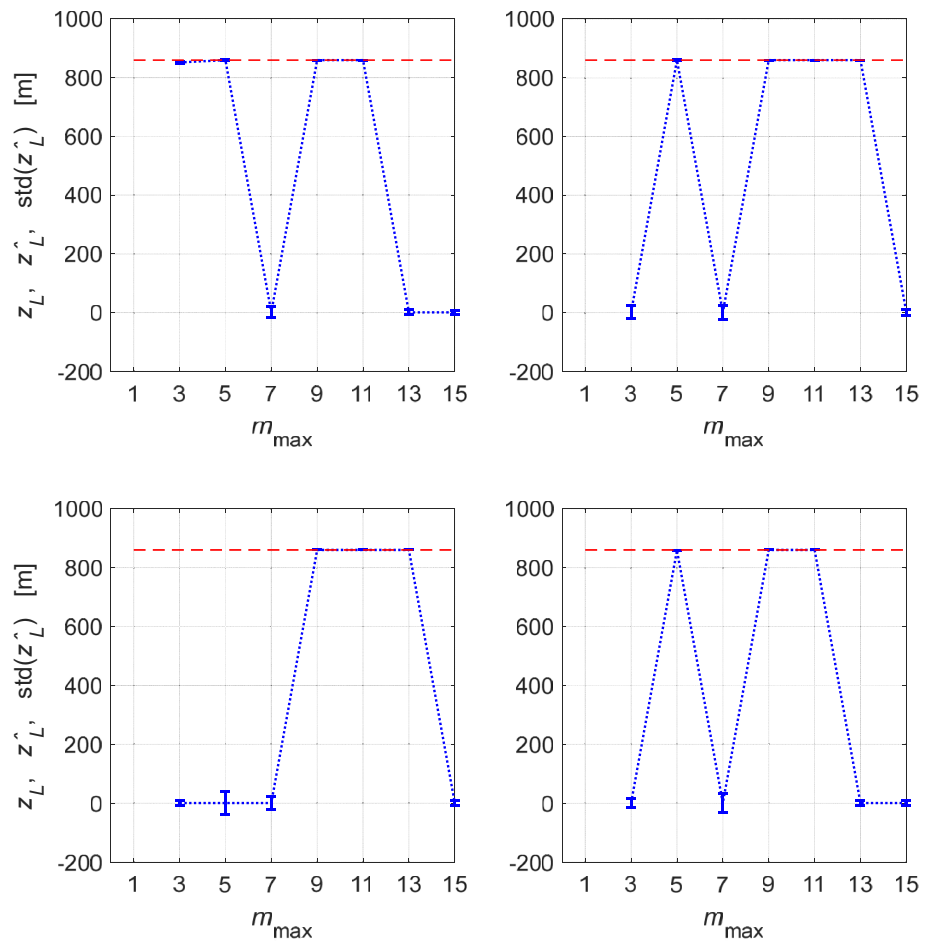


**Figure 9.** Localization results using different signal bandwidths indicated in the horizontal axis. Each graph provides several localizations using noisy measurement data set as a random realization of a transient event. The dashed red line corresponds to the actual leak location.

The two case studies reveal that the measurement errors lead to different levels of localization error depending upon the leak locations, and consequently, an appropriate number of resonant frequencies need to be incorporated to find leaks.

### 6.1. The Single Leak Case

An attractive leak detection experiment carried out in the Water Engineering Laboratory of the University of Perugia (Keramat & Duan, 2021; Keramat et al., 2019; X. Wang, Lin, et al., 2019; X. Wang, Palomar, et al., 2019) is inspected considering the theories developed in this research. To this end, the leak identification and corresponding uncertainties for different signal bandwidths are compared to interpret the flowchart in Figure 10.

The localization and corresponding uncertainty quantification of a single leak with effective area  $68 \text{ mm}^2$  placed at  $z_L = 60.84 \text{ m}$  from the upstream tank in an HDPE pipeline with length  $L = 166.28 \text{ m}$  is of interest. Other system specifications, including the calibrated creep coefficients, are given in Table 2. The viscoelastic parameters ( $\tau_k, J_k, k = 1, 2, 3$ ) in the table enable calculating the frequency-dependent wave speed (Brunone et al., 2018), and the unsteady friction is neglected in the transient model as discussed by X. Wang, Lin, et al. (2019) and X. Wang, Palomar, et al. (2019). The collected transient data following the complete closure of the downstream valve in  $T_c = 0.073 \text{ s}$  in the time and the frequency domain are respectively shown in Figures 11a and 11b. The process of obtaining the frequency spectra from the time histories is available in

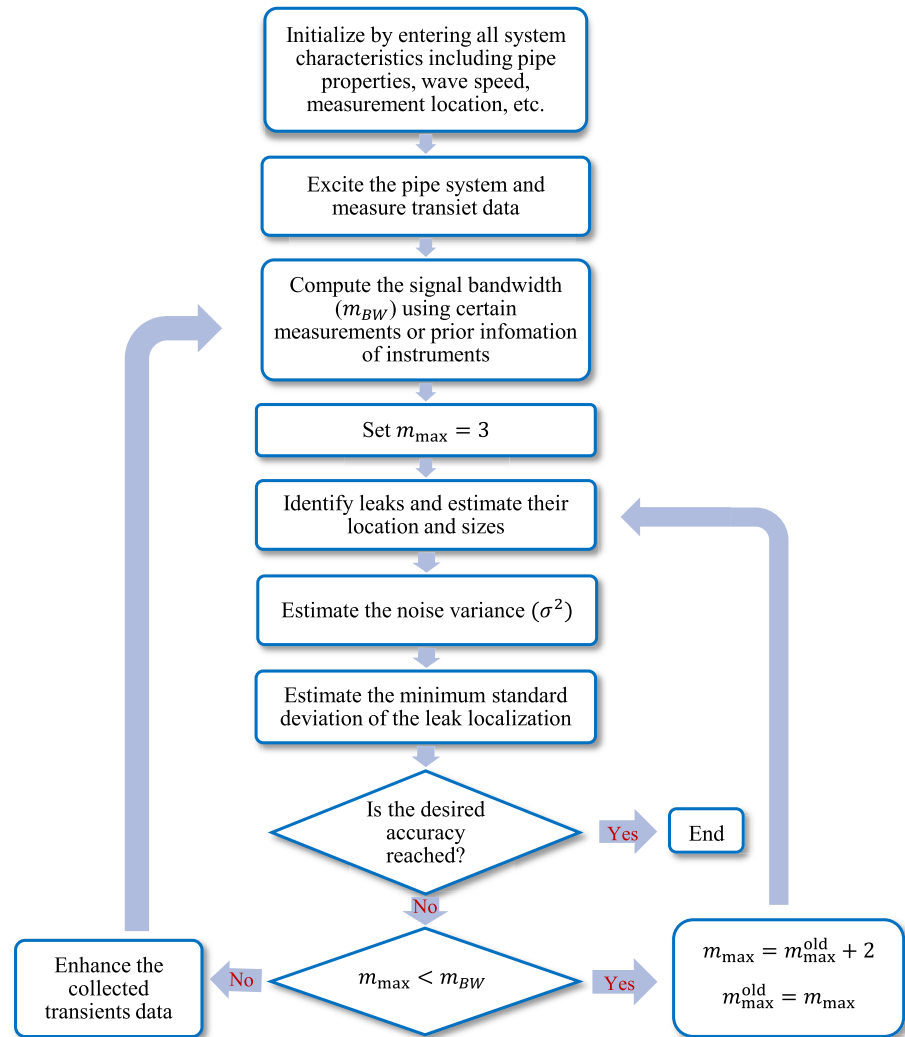


**Figure 10.** The proposed flowchart for the efficient application of resonant frequencies in a noisy environment.

many studies (e.g., Keramat et al., 2020). An inspection of the acquired frequency spectrum reveals that higher frequencies are much noisier than lower ones, and that  $m_{BW} \approx 19$  because after that, the noise traces seem to be more significant than the signatures of the system. For this bandwidth, the minimum reliable wavelength is  $\lambda_{\min} = 2\pi a/\omega = 2\pi a/(19\omega_{th}) = 31.54$  m. Accordingly, considering the Nyquist-Shannon sampling theory, half of this quantity (i.e.,  $\frac{31.54}{2} = 15.77$  m) is the resolution limit, which means resolving beyond this limit is super-resolution as seen in the current case.

According to the proposed approach, only the resonant frequencies are utilized (Lee et al., 2013, 2007, 2005). The results of the localization for different signal bandwidths are reported in Figures 12a–12h, which

**Table 2**

*Pipe and Flow Specifications of the Perugia Experiment (Keramat et al., 2019; X. Wang, Lin, et al., 2019; X. Wang, Palomar, et al., 2019)*

$D = 93.3$ mm	$J_0 = 0.68 \times 10^{-9} \text{Pa}^{-1}$	$\tau_1 = 0.05$ s	$J_1 = 1.061 \times 10^{-10} \text{Pa}^{-1}$
$\tau_2 = 0.5$ s	$J_2 = 1.05 \times 10^{-10} \text{Pa}^{-1}$	$\tau_3 = 1.5$ s	$J_3 = 0.905 \times 10^{-10} \text{Pa}^{-1}$
$e = 7.5$ mm	$\nu = 0.43$	$\rho = 1000$ kg/m <sup>3</sup>	$K = 2.1$ GPa
$Q_0 = 4.75$ L/s	$H_T = 18.28$ m	$a = 374.2$ m/s	$Q_{0L} = 1.28$ L/s

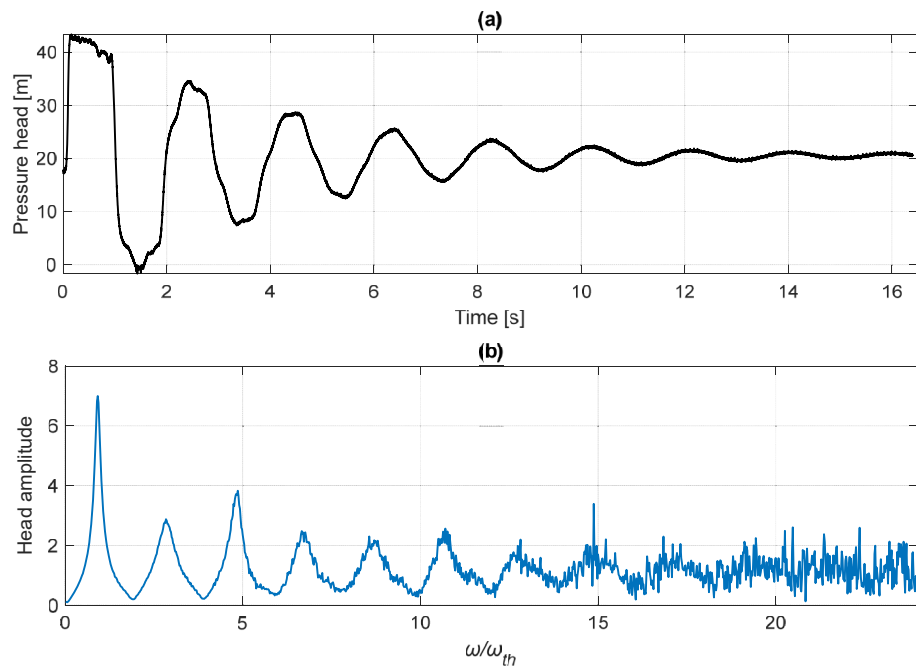


**Figure 11.** Measurements of pressure head at the downstream valve in the Perugia experiment; (a) time domain, and (b) frequency domain data.

correspond to (a)  $m_{\max} = 5$ , (b)  $m_{\max} = 7$ , (c)  $m_{\max} = 9$ , (d)  $m_{\max} = 11$ , (e)  $m_{\max} = 13$ , (f)  $m_{\max} = 15$ , (g)  $m_{\max} = 17$ , and (h)  $m_{\max} = 19$ . In Figure 13a, the identified locations and the estimated uncertainties versus the used signal bandwidths are summarized, where the dashed line shows the actual location of the leak. Furthermore, the standard deviations in this figure are plotted again in Figure 13b to clarify their trend versus the incorporated signal bandwidth. The reason behind the increased localization uncertainty for high signal bandwidths is the raised noise level at higher frequencies, as can be observed in Figure 11. Figure 13b suggests that signals with  $m_{\max} = 9, 11, 13, 15$  are able to provide satisfactory results but employing higher frequencies such as  $m_{\max} = 17, 19$  incorporate noise in the localization process significantly, thus leading to potential localization inaccuracy. Nevertheless, the estimated errors in all identifications are minimal in view of the Nyquist-Shannon resolution theory. Note that this is a single realization of the transient event, so no general conclusion can be drawn on the statistical properties of the identification. However, one may speculate that the noise absorbed in the simulation resulting from using high frequencies deteriorates the information gained about the system.

Considering the leak location and the pipe length,  $\frac{z_L}{L} = \frac{60.84}{166.28} \approx \frac{4}{11}$ , so that  $m_{\max} = 11$  is approximately the best choice for the bandwidth to be used in the localization scheme. This is also consistent with the results shown in Figures 12 and 13 in which for  $m_{\max} = 11$  reveal more accuracy. Although identifying each leak location requires a specific number of resonant frequencies, more frequencies will still solve the problem and pinpoint the leak. However, more frequencies than the required ones are prone to involving more noise in the simulation. That is why, as noted, for higher frequencies than  $m_{\max} = 11$ , the localization becomes unstable and continuously hops around the actual location, as seen in Figure 13a. The proposed error estimation approach aims to address the challenge of finding the required number of frequencies.

The estimated errors based on the proposed approach in inequality (Equation 2) is tiny in all cases for  $m_{\max} \geq 5$ . The reason is explained in detail now. First, note that any location with infinitesimal error for a specific bandwidth will remain in other higher bandwidths. For example, for  $m_{\max} = 7$ , the union of these locations  $\left\{\frac{2}{3}\right\} \cup \left\{\frac{2}{5}, \frac{4}{5}\right\}$  (which are for  $m_{\max} = 5$ ) and  $\left\{\frac{2}{7}, \frac{4}{7}, \frac{6}{7}\right\}$  are of minimal error and hence high accuracy, as shown in Figures 6

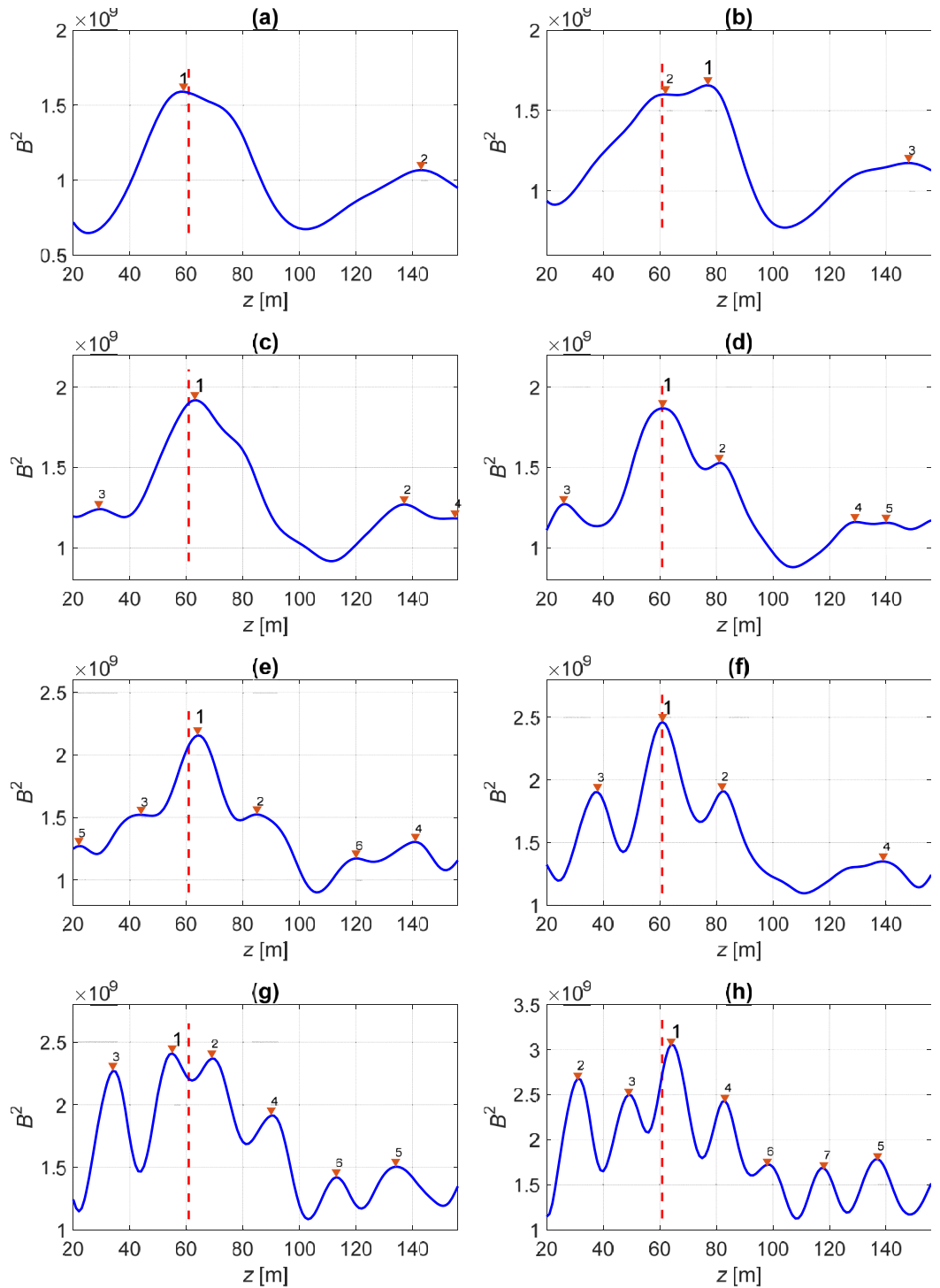


**Figure 12.** Localization results for the Perugia experiment corresponding to different signal bandwidths: (a)  $m_{\max} = 5$ , (b)  $m_{\max} = 7$ , (c)  $m_{\max} = 9$ , (d)  $m_{\max} = 11$ , (e)  $m_{\max} = 13$ , (f)  $m_{\max} = 15$ , (g)  $m_{\max} = 17$ , and (h)  $m_{\max} = 19$ .

and 7 for a 2,000 m pipeline. Second, in this experiment, the actual leak location is also close to  $z_L^* = \frac{2L}{5}$  with difference  $|z_L^* - z_L| = |0.4 \times 166.28 - 60.84| = 5.67$  m. That means this specific location is also close to that of minimum-error points corresponding to the bandwidth  $m_{\max} = 5$ . Accordingly, for all  $m_{\max} \geq 5$ , the error will be slight, as observed in Figure 13b.

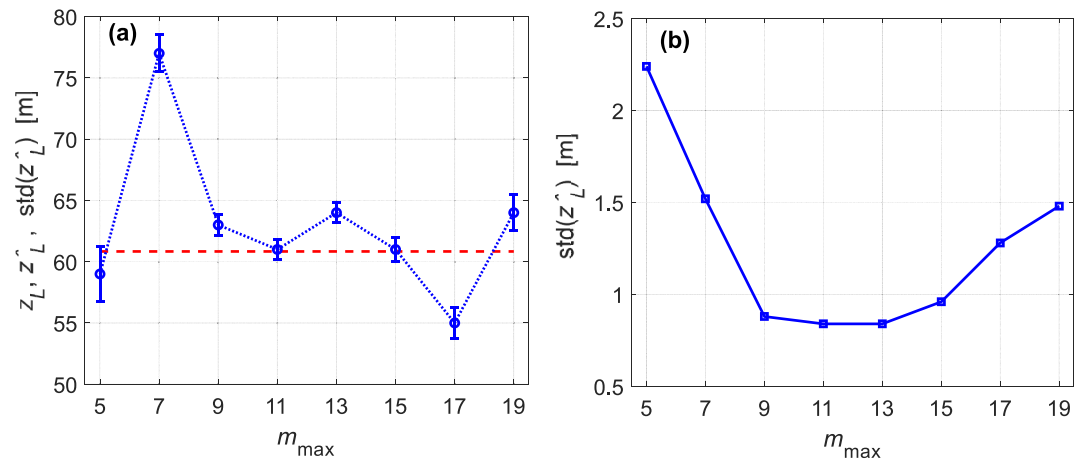


**Figure 13.** (a) The summary of the localization results and corresponding errors using different signal bandwidths indicated in the horizontal axis in the Perugia test. The dashed red line corresponds to the actual leak location. (b) The estimated lower bound standard deviation (CRLB) for different signal bandwidths.

### 6.2. The Double Leak Case

The formulations of localization uncertainty in this research are robust to multiple leak problems; thus, a double leak experiment is assessed here to realize the usefulness of the theories in a more complex localization problem.

The experiment conducted at the hydraulic laboratory of the Shahid Chamran University of Ahvaz consists of a reservoir-pipe-valve system with two leaks of the effective area  $A_{e1} = 19.8 \text{ mm}^2$ ,  $A_{e2} = 11.5 \text{ mm}^2$  placed at  $z_{L1} = 56.3 \text{ m}$ ,  $z_{L2} = 117.4 \text{ m}$  from the upstream tank in an HDPE pipeline with the length  $L = 158 \text{ m}$  (Rezpour et al., 2021). Other specifications, including the calibrated viscoelastic parameters and wave speed, are shown in Table 3, and the experimental water hammer pressures in the time and the frequency domain following the full closure of the downstream valve are depicted in Figures 14a and 14b, respectively.

For this experiment, two studies are conducted to realize the research merits in the transient-based assessment and localization. First, the localization uncertainties for all possible double leaks cases in the pipeline are calculated, and second, the uncertainties corresponding to several signal bandwidths are computed, as explained in the following.

We consider all double leak scenarios throughout the domain and compute the localization uncertainties of each one based on  $m_{\max} = 5$  used as the signal bandwidth. The estimated lower bound standard deviations are plotted in Figures 15a and 15b for the first and second leak, respectively. These graphs give valuable insights into the level of localization error one may get given the estimated leak locations. For example, the result corresponding to the actual leak location (indicated by the red cross) implies that even if the estimated site falls precisely at the real leak location, the estimation is still subject to the calculated uncertainty.

As learned from the previous experiment, large noise levels at higher modes deteriorate the localization performance. To further elaborate on this notion for double leaks, the noise levels on the measured frequency response function ( $\mathbf{h}^M$ ) corresponding to different signal bandwidths ( $m_{\max}$ ) are plotted in Figure 16a. They are estimated using:

$$\sigma(m_{\max}) = \sqrt{\frac{1}{N-1} (\mathbf{h}^M - \mathbf{h})^H (\mathbf{h}^M - \mathbf{h})} = \sigma_n, \quad (20)$$

**Table 3**  
The Details of the Double Leaks Case in the Shahid Chamran Experiment (Rezpour et al., 2021)

$D = 50.5 \text{ mm}$	$J_0 = 0.88 \times 10^{-9} \text{ Pa}^{-1}$	$\tau_1 = 0.014 \text{ s}$	$J_1 = 0.477 \times 10^{-10} \text{ Pa}^{-1}$
$\tau_2 = 0.13 \text{ s}$	$J_2 = 1.124 \times 10^{-10} \text{ Pa}^{-1}$	$\tau_3 = 1.38 \text{ s}$	$J_3 = 1.422 \times 10^{-10} \text{ Pa}^{-1}$
$e = 6.5 \text{ mm}$	$\nu = 0.43$	$\rho = 1,000 \text{ kg/m}^3$	$K = 2.1 \text{ GPa}$
$Q_0 = 0.95 \text{ L/s}$	$H_T = 41.7 \text{ m}$	$a = 406 \text{ m/s}$	$f = 0.02$

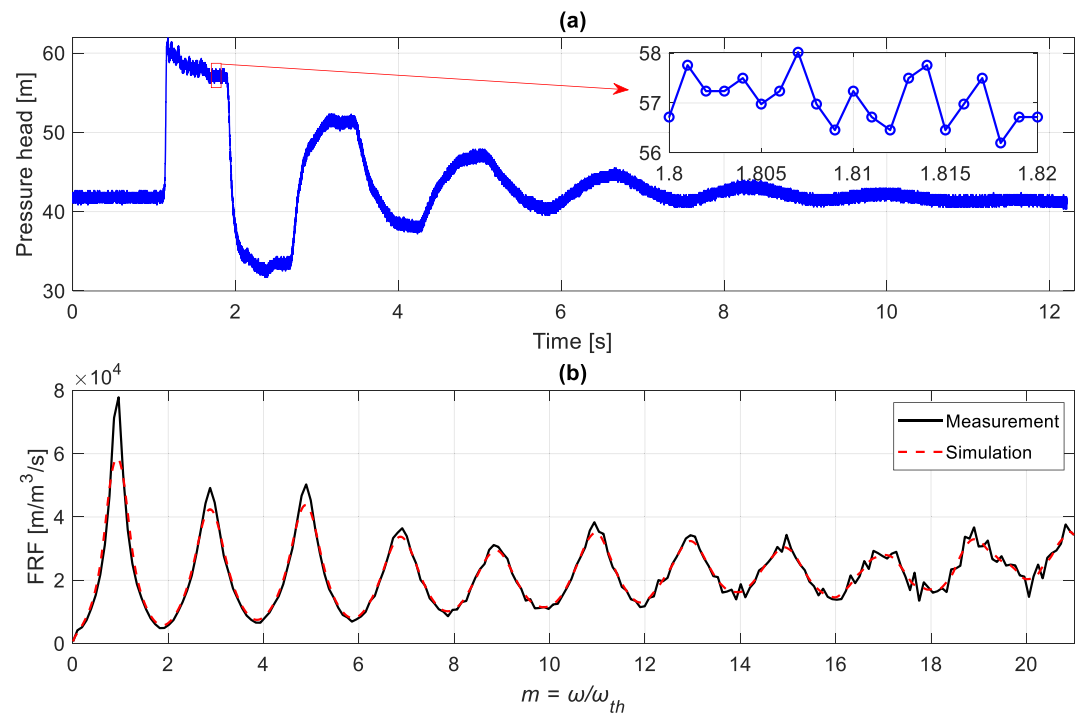


**Figure 14.** Measurements of pressure head at the downstream valve in the Shahid Chamran experiment; (a) collected pressure data in the time domain, and (b) measured (continuous black) and simulated (dashed red) data in the frequency domain.

where  $\mathbf{h}$  represents the computed response function, and  $N$  indicates its length (sample size), as discussed in Equation 5. As realized in Figure 16a and also observed in Figure 14b, the noise level ( $\sigma_n$ ) rises with the bandwidth, thus calling for an appropriate number of resonant frequencies to be used for the localization. This is acquired via the uncertainties estimated using the proposed formulations, as depicted for various signals in Figure 16b. The optimum bandwidth is suggested to be  $m_{\max} = 9$ , based on the estimated CRLBs, as shown in Figure 16b. To plot the results in Figure 16, first, localization is carried out based on a given quantity for  $m_{\max}$ , then the noise level corresponding to that signal bandwidth is evaluated using Equation 20, allowing for estimating the uncertainties drawn in inequality (Equation 2). Interested readers in details of the localization are referred to the Keramat et al. (2022). The application of  $m_{\max} = 9$  in the localization guarantees minimum noise involvement in the process.

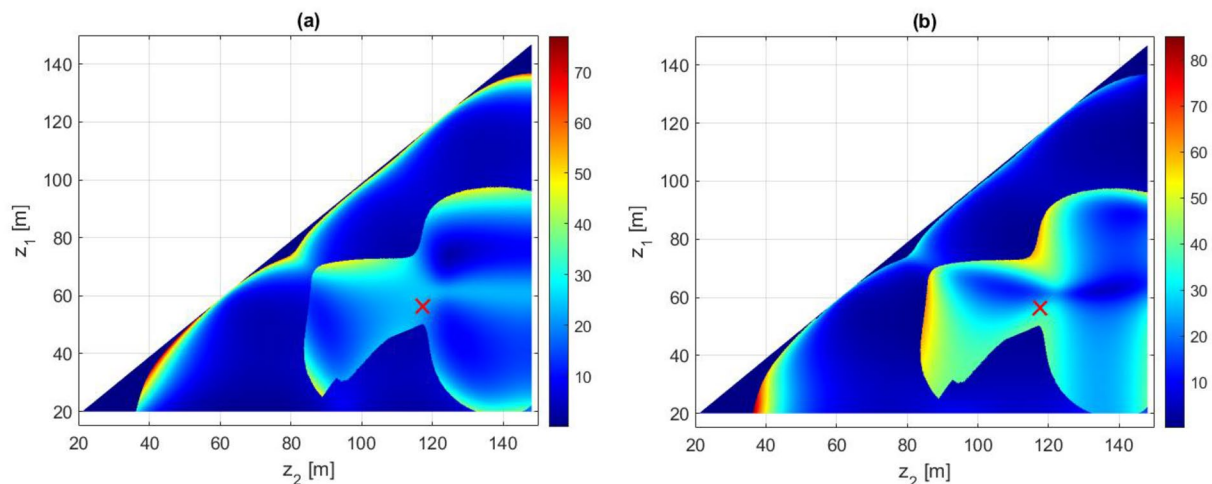


**Figure 15.** Localization uncertainties of the first (a) and second leak (b) for all possible leak locations along the pipeline. The bandwidth of the used signal is set to  $\omega_{\max}/\omega_{th} = m_{\max} = 5$ .

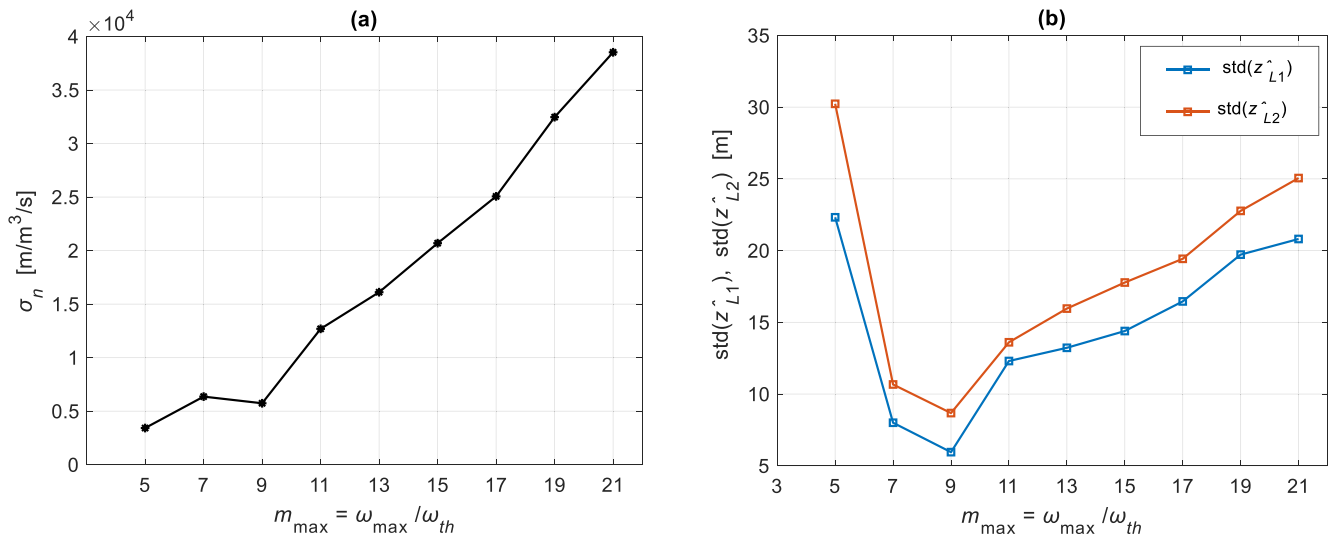


**Figure 16.** (a) Estimated noise standard deviations corresponding to various signals used in localization. (b) Evaluated lower bounds localizations of the first (blue) and second leak (orange) for various signal bandwidths.

## 7. Conclusions

In this research, the lower bound of the covariance matrix of leak parameters was estimated based on the CRLB theory. This lower bound implied the minimum mean square error of the estimated leak sizes and locations. The findings were plotted mostly as error versus potential-leak space curves to draw complementary reports on the identification outcomes. Readily illustrated and verified, the error-space graphs present helpful supplements on detectability to be used in the actual practice of leak detection in a simple pipeline system. The key findings in this regard are listed as follows:

- Corresponding to any specific bandwidth of the signal incorporated in the identification, there are some distinct points at the pipeline in which the estimated error is minimal. It is advised to locate them before the leak detection since the procedure to find them is straightforward.
- Apart from the above-mentioned nodes, the error-space graphs provide quantitative estimates of localization uncertainty.
- Based on the proposed error-location curves for a given signal and noise variance, one may design a strategy for the localization practice within the desired accuracy: if the maximum error estimate is lower than the desired one, then the facility and the corresponding methodology are acceptable otherwise further actions are recommended, for example, conducting more experiments to attain signals with higher bandwidth or lower noise level or using better instruments.
- The proposed error estimate formulas allow reporting the estimation error corresponding to the localization results. With this, one can use the minimum number of resonant frequencies to reduce the noise impacts on the localization.

## Appendix A: Evaluation of the Fisher Information Matrix Elements

Considering Equation 9, the second derivative of the likelihood function with respect to the leak locations is expanded as follows

$$\begin{aligned} \frac{\partial^2 \ln L}{\partial z_i^2} &= -\frac{1}{\sigma^2} \frac{\partial^2}{\partial z_i^2} \|\mathbf{h}^M - \mathbf{h}\|^2 = -\frac{1}{\sigma^2} \frac{\partial^2}{\partial z_i^2} (\mathbf{h}^M - \mathbf{h})^H (\mathbf{h}^M - \mathbf{h}) = -\frac{1}{\sigma^2} \left( -\mathbf{h}^{M^H} \frac{\partial^2 \mathbf{h}}{\partial z_i^2} - \frac{\partial^2 \mathbf{h}^H}{\partial z_i^2} \mathbf{h}^M + \frac{\partial^2 (\mathbf{h}^H \mathbf{h})}{\partial z_i^2} \right) \\ &= -\frac{1}{\sigma^2} \left( -\mathbf{h}^{M^H} \frac{\partial^2 \mathbf{h}}{\partial z_i^2} - \frac{\partial^2 \mathbf{h}^H}{\partial z_i^2} \mathbf{h}^M + \frac{\partial^2 \mathbf{h}^H}{\partial z_i^2} \mathbf{h} + 2 \frac{\partial \mathbf{h}^H}{\partial z_i} \frac{\partial \mathbf{h}}{\partial z_i} + \mathbf{h}^H \frac{\partial^2 \mathbf{h}}{\partial z_i^2} \right), \end{aligned} \quad (\text{A1})$$

which after the application of the expectation and considering Equation 3 can be simplified to:

$$-\mathbb{E} \left[ \frac{\partial^2 \ln L}{\partial z_i^2} \right] = \frac{1}{\sigma^2} \mathbb{E} \left[ \frac{\partial^2}{\partial z_i^2} \|\mathbf{h}^M - \mathbf{h}\|^2 \right] = \frac{2}{\sigma^2} \left( \frac{\partial \mathbf{h}^H}{\partial z_i} \frac{\partial \mathbf{h}}{\partial z_i} \right) = \frac{2}{\sigma^2} \left\| \frac{\partial \mathbf{h}}{\partial z_i} \right\|^2 \quad (\text{A2})$$

Once the derivative operator applies to two different leak locations, the matrix entries reduce to:

$$\begin{aligned} -\mathbb{E} \left[ \frac{\partial^2 \ln L}{\partial z_i \partial z_j} \right] &= \frac{1}{\sigma^2} \mathbb{E} \left[ \frac{\partial^2}{\partial z_i \partial z_j} \|\mathbf{h}^M - \mathbf{h}\|^2 \right] = \frac{1}{\sigma^2} \mathbb{E} \left[ \frac{\partial^2}{\partial z_i \partial z_j} \left( \mathbf{h}^{M^H} \mathbf{h}^M - \mathbf{h}^{M^H} \mathbf{h} - \mathbf{h}^H \mathbf{h}^M + \mathbf{h}^H \mathbf{h} \right) \right] \\ &= \frac{1}{\sigma^2} \mathbb{E} \left[ -\mathbf{h}^{M^H} \frac{\partial^2 \mathbf{h}}{\partial z_i \partial z_j} - \frac{\partial^2 \mathbf{h}^H}{\partial z_i \partial z_j} \mathbf{h}^M + \mathbf{h}^H \frac{\partial^2 \mathbf{h}}{\partial z_i \partial z_j} + \frac{\partial^2 \mathbf{h}^H}{\partial z_i \partial z_j} \mathbf{h} + \frac{\partial \mathbf{h}^H}{\partial z_j} \frac{\partial \mathbf{h}}{\partial z_i} + \frac{\partial \mathbf{h}^H}{\partial z_i} \frac{\partial \mathbf{h}}{\partial z_j} \right] \\ &= \frac{1}{\sigma^2} \left( \frac{\partial \mathbf{h}^H}{\partial z_j} \frac{\partial \mathbf{h}}{\partial z_i} + \frac{\partial \mathbf{h}^H}{\partial z_i} \frac{\partial \mathbf{h}}{\partial z_j} \right), \end{aligned} \quad (\text{A3})$$

The correlation between leak location and leak size is quantified using:

$$-\mathbb{E} \left[ \frac{\partial^2 \ln L}{\partial z_i \partial \alpha_j} \right] = \frac{1}{\sigma^2} \left( \frac{\partial \mathbf{h}^H}{\partial \alpha_j} \frac{\partial \mathbf{h}}{\partial z_i} + \frac{\partial \mathbf{h}^H}{\partial z_i} \frac{\partial \mathbf{h}}{\partial \alpha_j} \right) \quad (\text{A4})$$

Likewise, the variance and covariance of leak sizes respectively require estimating

$$-\mathbb{E} \left[ \frac{\partial^2 \ln L}{\partial \alpha_i^2} \right] = \frac{2}{\sigma^2} \left( \frac{\partial \mathbf{h}^H}{\partial \alpha_i} \frac{\partial \mathbf{h}}{\partial \alpha_i} \right) = \frac{2}{\sigma^2} \left\| \frac{\partial \mathbf{h}}{\partial \alpha_i} \right\|^2 \quad (\text{A5})$$

and

$$-\mathbb{E} \left[ \frac{\partial^2 \ln L}{\partial \alpha_i \partial \alpha_j} \right] = \frac{1}{\sigma^2} \left( \frac{\partial \mathbf{h}^H}{\partial \alpha_j} \frac{\partial \mathbf{h}}{\partial \alpha_i} + \frac{\partial \mathbf{h}^H}{\partial \alpha_i} \frac{\partial \mathbf{h}}{\partial \alpha_j} \right), \quad (\text{A6})$$

Note that in Equations 23, 24, and 26, since the real part of the resultant value is of interest, the property  $\Re(Z_1^H Z_2) = \Re(Z_2^H Z_1)$ , where  $Z_1 Z_2$  belong to sets of complex numbers, applies which eventually allows for the representation in inequality (Equation 2).

## Appendix B: Another Derivation of the CRLB Through the Taylor Series

The second approach adopts the basic knowledge of mathematics; hence it may be considered intuitive proof for the former process. Consider the first-order Taylor approximation of the measurements  $\mathbf{h}^M$  about the true values  $\theta = (\mathbf{z}_L; \alpha_L)$  defined in Equation 1, we have (e.g., Lambert, 2012):

$$\mathbf{h}^M = \mathbf{h}(\theta) + \frac{\partial \mathbf{h}}{\partial \theta} (\hat{\theta} - \theta) + \varepsilon \text{ or } \mathbf{h}^M - \mathbf{h}(\theta) = \frac{\partial \mathbf{h}}{\partial \theta} (\hat{\theta} - \theta) + \varepsilon, \quad (\text{B1})$$

where  $\varepsilon$  stands for the error vector of size  $(N_s, J)$ . If each side of the resultant expression in Equation 27 is multiplied by its conjugate transpose, then after the application of the expectation, we have:

$$\begin{aligned} \mathbb{E} \left[ (\mathbf{h}^M - \mathbf{h}) (\mathbf{h}^M - \mathbf{h})^H \right] &\geq \mathbb{E} \left[ \frac{\partial \mathbf{h}}{\partial \theta} (\hat{\theta} - \theta) \left( \frac{\partial \mathbf{h}}{\partial \theta} (\hat{\theta} - \theta) \right)^H \right] \Rightarrow \\ \Sigma(\mathbf{h}^M) &= \sigma^2 \mathbf{I}_{N_s, J} \geq \mathbb{E} \left[ \frac{\partial \mathbf{h}}{\partial \theta} (\hat{\theta} - \theta) (\hat{\theta} - \theta)^H \frac{\partial \mathbf{h}^H}{\partial \theta} \right] \Rightarrow \\ \sigma^2 \mathbf{I}_{N_s, J} &\geq \left( \frac{\partial \mathbf{h}}{\partial \theta} \Sigma(\hat{\theta}) \frac{\partial \mathbf{h}^H}{\partial \theta} \right) \Rightarrow \text{cov}(\hat{\theta}) = \frac{\sigma^2}{2} \left( \Re \left( \frac{\partial \mathbf{h}^H}{\partial \theta} \frac{\partial \mathbf{h}}{\partial \theta} \right) \right)^{-1} \leq \Sigma(\hat{\theta}) \end{aligned} \quad (\text{B2})$$

This formula is consistent with inequality (Equation 2).

### Appendix C: Analytical Expressions of Equation 13

For the case of a single leak with leak location  $z_L$  and size  $\alpha_L$ , the derivative of the head amplitudes corresponding to each frequency can be analytically evaluated:

$$\begin{aligned} \frac{\partial h}{\partial z_L} &= \frac{\partial}{\partial z_L} \left( \frac{m_{21}^{NLm} + \alpha_L m_{21}^{SLm}}{m_{11}^{NLD} + \alpha_L m_{11}^{SLD}} \right) \\ &= \frac{\alpha_L \frac{\partial m_{21}^{SLm}}{\partial z_L} (m_{11}^{NLD} + \alpha_L m_{11}^{SLD}) - \alpha_L \frac{\partial m_{11}^{SLD}}{\partial z_L} (m_{21}^{NLm} + \alpha_L m_{21}^{SLm})}{(m_{11}^{NLD} + \alpha_L m_{11}^{SLD})^2} \end{aligned} \quad (C1)$$

and

$$\begin{aligned} \frac{\partial h}{\partial \alpha_L} &= \frac{\partial}{\partial \alpha_L} \left( \frac{m_{21}^{NLm} + \alpha_L m_{21}^{SLm}}{m_{11}^{NLD} + \alpha_L m_{11}^{SLD}} \right) \\ &= \frac{m_{21}^{SLm} (m_{11}^{NLD} + \alpha_L m_{11}^{SLD}) - m_{11}^{SLD} (m_{21}^{NLm} + \alpha_L m_{21}^{SLm})}{(m_{11}^{NLD} + \alpha_L m_{11}^{SLD})^2} \end{aligned} \quad (C2)$$

in which the relations of each statement in these equations can be found in Equation 11, and the required derivatives are determined as follows:

$$\frac{\partial m_{21}^{SLm}}{\partial z_L} = \vartheta^2 \mu \sinh(\mu(z_m - 2z_L)) \quad (C3)$$

and

$$\frac{\partial m_{11}^{SLD}}{\partial z_L} = -\vartheta \mu \cosh(\mu(L - 2z_L)) \quad (C4)$$

### Nomenclature

<b>b</b>	Right-hand side vector being a function of measurements
<b>F<sub>θ</sub></b>	The Fisher information matrix
<b>h</b>	Computed pressure head
<b>h<sup>M</sup></b>	measured pressure head
<b>G</b>	Coefficient matrix being a function of leak locations
<b>n</b>	Noise vector
<b>ẑ</b>	Estimated leak locations
<b>α̂</b>	Estimated leak sizes
<b>θ = (z<sub>L</sub>; α<sub>L</sub>)</b>	Parameters of the leak detection problem
<b>a</b>	Pressure wave speed
<b>h</b>	Pressure head amplitude
<b>J</b>	Number of entries of the measurement vector
<b>m</b>	Elements of the transfer matrix
<b>ρ</b>	Density
<b>s</b>	Laplace variable
<b>z</b>	Axial coordinate of pipe
<b>q</b>	Cross-sectional flow rate
<b>g</b>	Gravitational acceleration
<b>D</b>	Inner diameter of the pipe
<b>e</b>	Pipe wall thickness
<b>t</b>	Time
<b>f</b>	Friction factor
<b>α<sub>L</sub></b>	Characteristic leak size
<b>z<sub>L</sub></b>	Leak location coordinate

$E$	Elastic modulus of the pipe wall
$j$	Frequency index
$m$	Measurement-station node
$k$	Data index
$D$	Downstream node
NL	No leak
SL	Single leak
H	Conjugate transpose
U	Upstream node
CRLB =	Cramer Rao Lower Bound
MLE =	Maximum Likelihood Estimation
RMSE =	Root Mean Square Error
SNR =	Signal to Noise Ratio
VE =	Viscoelasticity

### Conflict of Interest

The authors declare no conflicts of interest relevant to this study.

### Data Availability Statement

All essential data sets for this research are available at <https://doi.org/10.5281/zenodo.6413965>.

### Acknowledgments

This work has been supported by the Hong Kong Research Grants Council (RGC) Projects (Grants 15200719 and 15201017). The University of Perugia is acknowledged for the experimental data used in Section 6.

### References

- Alawadhi, A., & Tartakovsky, D. M. (2020). Bayesian update and method of distributions: Application to leak detection in transmission mains. *Water Resources Research*, 56(2), e2019WR025879. <https://doi.org/10.1029/2019wr025879>
- Asada, Y., Kimura, M., Azechi, I., Iida, T., & Kubo, N. (2020). Transient damping method for narrowing down leak location in pressurized pipelines. *Hydrological Research Letters*, 14(1), 41–47. <https://doi.org/10.3178/hrl.14.41>
- Brunone, B. (1999). Transient test-based technique for leak detection in outfall pipes. *Journal of Water Resources Planning and Management*, 125(5), 302–306. [https://doi.org/10.1061/\(asce\)0733-9496\(1999\)125:5\(302\)](https://doi.org/10.1061/(asce)0733-9496(1999)125:5(302))
- Brunone, B., Ferrante, M., & Meniconi, S. (2008). Portable pressure wave-maker for leak detection and pipe system characterization. *American Water Works Association*, 100(4), 108–116. <https://doi.org/10.1002/j.1551-8833.2008.tb09607.x>
- Brunone, B., Meniconi, S., & Capponi, C. (2018). Numerical analysis of the transient pressure damping in a single polymeric pipe with a leak. *Urban Water Journal*, 15(8), 760–768. <https://doi.org/10.1080/1573062x.2018.1547772>
- Casella, G., & Berger, R. L. (2002). *Statistical inference* (2nd ed.). Duxbury/Thomson Learning.
- Chaudhry, M. H. (2014). *Applied hydraulic transients* (3rd ed.). Springer.
- Che, T. C., Duan, H. F., & Lee, P. J. (2021). Transient wave-based methods for anomaly detection in fluid pipes: A review. *Mechanical Systems and Signal Processing*, 160, 107874. <https://doi.org/10.1016/j.ymssp.2021.107874>
- Colombo, A. F., Lee, P., & Karney, B. W. (2009). A selective literature review of transient-based leak detection methods. *Journal of Hydro-Environment Research*, 2(4), 212–227. <https://doi.org/10.1016/j.jher.2009.02.003>
- Covas, D., & Ramos, H. (2010). Case studies of leak detection and location in water pipe systems by inverse transient analysis. *Journal of Water Resources Planning and Management*, 136(2), 248–257. [https://doi.org/10.1061/\(asce\)0733-9496\(2010\)136:2\(248\)](https://doi.org/10.1061/(asce)0733-9496(2010)136:2(248))
- Diong, M. L., Roueff, A., Lasaygues, P., & Litman, A. (2015). Precision analysis based on Cramer-Rao bound for 2D acoustics and electromagnetic inverse scattering. *Inverse Problems*, 31(7), 075003. <https://doi.org/10.1088/0266-5611/31/7/075003>
- Du, X., Lambert, M. F., Chen, L., Hu, E. J., & Xi, W. (2020). Pipe burst detection, localization, and quantification using the transient pressure damping method. *Journal of Hydraulic Engineering*, 146(11), 4020077. [https://doi.org/10.1061/\(ASCE\)HY.1943-7900.0001810](https://doi.org/10.1061/(ASCE)HY.1943-7900.0001810)
- Du, X., Zeng, W., Lambert, M. F., Chen, L., & Hu, E. J. (2021). Approach for near-real-time pipe burst detection, localization, and quantification with low data transmission and sampling rates. *Journal of Water Resources Planning and Management*, 147(7). [https://doi.org/10.1061/\(ASCE\)WR.1943-5452.0001380](https://doi.org/10.1061/(ASCE)WR.1943-5452.0001380)
- Duan, H. F. (2016). Sensitivity analysis of a transient-based frequency domain method for extended blockage detection in water pipeline systems. *Journal of Water Resources Planning and Management*, 142(4), 04015073. [https://doi.org/10.1061/\(asce\)wr.1943-5452.0000625](https://doi.org/10.1061/(asce)wr.1943-5452.0000625)
- Duan, H. F. (2017). Transient frequency response based leak detection in water supply pipeline systems with branched and looped junctions. *Journal of Hydroinformatics*, 19(1), 17–30. <https://doi.org/10.2166/hydro.2016.008>
- Duan, H. F. (2018). Accuracy and sensitivity evaluation of TFR method for leak detection in multiple pipeline water supply systems. *Water Resources Management*, 32, 2147–2164. <https://doi.org/10.1007/s11269-018-1923-7>
- Duan, H. F., Pan, B., Wang, M. L., Chen, L., Zheng, F. F., & Zhang, Y. (2020). State-of-the-art review on the transient flow modeling and utilization for urban water supply system (UWSS) management. *Journal of Water Supply: Research & Technology—Aqua*, 69(8), 858–893. <https://doi.org/10.2166/aqua.2020.048>
- Ferrante, M., Brunone, B., & Meniconi, S. (2007). Wavelets for the analysis of transient pressure signals for leak detection. *Journal of Hydraulic Engineering*, 133(11), 1274–1282. [https://doi.org/10.1061/\(asce\)0733-9429\(2007\)133:11\(1274\)](https://doi.org/10.1061/(asce)0733-9429(2007)133:11(1274))
- Ferrante, M., Brunone, B., Meniconi, S., Karney, B. W., & Massari, C. (2014). Leak size, detectability and test conditions in pressurized pipe systems. *Water Resources Management*, 28, 4583–4598. <https://doi.org/10.1007/s11269-014-0752-6>

- Ferrante, M., Capponi, C., Collins, R., Edwards, J., Brunone, B., & Meniconi, S. (2016). Numerical transient analysis of random leakage in time and frequency domains. *Civil Engineering and Environmental Systems*, 33(1), 70–84. <https://doi.org/10.1080/10286608.2016.1138941>
- Gong, J., Lambert, M. F., Simpson, A. R., & Zecchin, A. C. (2013). Single-event leak detection in pipeline using first three resonant responses. *Journal of Hydraulic Engineering*, 139(6), 645–655. [https://doi.org/10.1061/\(ASCE\)HY.1943-7900.0000720](https://doi.org/10.1061/(ASCE)HY.1943-7900.0000720)
- Hastings, W. K. (1970). Monte Carlo sampling methods using Markov chains and their applications. *Biometrika*, 57(1), 97–109. ISSN 0006-3444. <https://doi.org/10.1093/biomet/57.1.97>
- Kapelan, Z., Savic, D. A., & Walters, G. A. (2003). A hybrid inverse transient model for leakage detection and roughness calibration in pipe networks. *Journal of Hydraulic Research*, 41(5), 481–492. <https://doi.org/10.1080/00221680309499993>
- Karimian, H. A., Ahmadi, A., & Keramat, A. (2020). Frequency response of water hammer with fluid-structure interaction in a viscoelastic pipe. *Mechanical Systems and Signal Processing*, 144, 106848. <https://doi.org/10.1016/j.ymsp.2020.106848>
- Kay, S. M. (1993). *Fundamentals of statistical signal processing, estimation theory* (Vol. 1). Prentice-Hall.
- Keramat, A., & Duan, H. F. (2021). Spectral-based pipeline leak detection using a single spatial measurement. *Mechanical Systems and Signal Processing*, 161, 107940. <https://doi.org/10.1016/j.ymsp.2021.107940>
- Keramat, A., & Haghighi, A. (2014). Straightforward transient-based approach for the creep function determination in viscoelastic pipes. *Journal of Hydraulic Engineering, ASCE*, 140(12), 04014058. [https://doi.org/10.1061/\(asce\)hy.1943-7900.0000929](https://doi.org/10.1061/(asce)hy.1943-7900.0000929)
- Keramat, A., & Zanganeh, R. (2019). Statistical performance analysis of transient-based extended blockage detection in a water supply pipeline. *Journal of Water Supply: Research & Technology—Aqua*, 68(5), 346–357. <https://doi.org/10.2166/aqua.2019.014>
- Keramat, A., Duan, H.-F., Pan, B., & Hou, Q. (2022). Gradient-based optimization for spectral-based multiple-leak identification. *Mechanical Systems and Signal Processing*, 171. <https://doi.org/10.1016/j.ymsp.2022.108840>
- Keramat, A., Fathi-Moghadam, M., Zanganeh, R., Rahmanshahi, M., Tijsseling, A. S., & Jabbari, E. (2020). Experimental investigation of transients-induced fluid-structure interaction in a pipeline with multiple-axial supports. *Journal of Fluids and Structures*, 93, 102848. <https://doi.org/10.1016/j.jfluidstructs.2019.102848>
- Keramat, A., Gaffarian Kolahi, A., & Ahmadi, A. (2014). Water hammer modeling of viscoelastic pipes with a time-dependent Poisson's ratio. *Journal of Fluids and Structures*, 43, 164–178.
- Keramat, A., Ghidaoui, M., Wang, X., & Louati, M. (2018). Cramer-Rao lower bound for performance analysis of leak detection. *Journal of Hydraulic Engineering, ASCE*, 145(6), 04019018.
- Keramat, A., Karney, B., Ghidaoui, M. S., & Wang, X. (2021). Transient-based leak detection in the frequency domain considering fluid-structure interaction and viscoelasticity. *Mechanical Systems and Signal Processing*, 153, 107500.
- Keramat, A., Louati, M., Wang, X., Meniconi, S., Brunone, B., & Ghidaoui, M. S. (2019). Objective functions for transient-based pipeline leakage detection in a noisy environment: Least square and matched-filter. *Journal of Water Resources Planning and Management, ASCE*, 145(10), 04019042. [https://doi.org/10.1061/\(asce\)wr.1943-5452.0001108](https://doi.org/10.1061/(asce)wr.1943-5452.0001108)
- Lambert, H. C. (2012). Cramer-rao bounds for target tracking problems involving colored measurement noise. *IEEE Transactions on Aerospace and Electronic Systems*, 48(1), 620–636. <https://doi.org/10.1109/TAES.2012.6129659>
- Lee, P. J., Duan, H. F., Ghidaoui, M., & Karney, B. (2013). Frequency domain analysis of pipe fluid transient behavior. *Journal of Hydraulic Research*, 51(6), 609–622. <https://doi.org/10.1080/00221686.2013.814597>
- Lee, P. J., Duan, H. F., Tuck, J., & Ghidaoui, M. (2015). Numerical and experimental study on the effect of signal bandwidth on pipe assessment using fluid transients. *Journal of Hydraulic Engineering, ASCE*, 141(2), 04014074. [https://doi.org/10.1061/\(ASCE\)HY.1943-7900.0000961](https://doi.org/10.1061/(ASCE)HY.1943-7900.0000961)
- Lee, P. J., Lambert, M. F., Simpson, A. R., Vitkovsky, J. P., & Misiunas, D. (2007). Leak location in single pipelines using transient reflections. *Australian Journal of Water Resources*, 11(1), 53–65. <https://doi.org/10.1080/13241583.2007.11465311>
- Lee, P. J., Vitkovsky, J. P., Lambert, M. F., Simpson, A. R., & Liggett, J. A. (2005). Frequency domain analysis for detecting pipeline leaks. *Journal of Hydraulic Engineering*, 131(7), 596–604. [https://doi.org/10.1061/\(asce\)0733-9429\(2005\)131:7\(596\)](https://doi.org/10.1061/(asce)0733-9429(2005)131:7(596))
- Liggett, J. A., & Chen, L.-C. (1994). Inverse transient analysis in pipe networks. *Journal of Hydraulic Engineering*, 1208, 934–955. [https://doi.org/10.1061/\(asce\)0733-9429\(1994\)120:8\(934\)](https://doi.org/10.1061/(asce)0733-9429(1994)120:8(934))
- Louati, M., Ghidaoui, M. S., Tekitek, M. M., & Lee, P. J. (2020). Wave-leak interaction in a simple pipe system. *Journal of Hydraulic Engineering, ASCE*, 146(4), 04020013. [https://doi.org/10.1061/\(asce\)hy.1943-7900.0001714](https://doi.org/10.1061/(asce)hy.1943-7900.0001714)
- Malekpour, A., & She, Y. (2021). Real-time leak detection in oil pipelines using an inverse transient analysis model. *Journal of Loss Prevention in the Process Industries*, 70, 104411. <https://doi.org/10.1016/j.jlp.2021.104411>
- Meniconi, S., Capponi, C., Frisinghelli, M., & Brunone, B. (2021). Leak detection in a real transmission main through transient tests: Deeds and misdeeds. *Water Resources Research*, 57(3), e2020WR027838. <https://doi.org/10.1029/2020wr027838>
- Mpesha, W., Gassman, S. L., & Chaudhry, M. H. (2011). Leak detection in pipes by frequency response method. *Journal of Hydraulic Engineering*, 127(2), 134–147.
- Nehorai, A., & Hawkes, M. (2000). Performance bounds for estimating vector systems. *IEEE Transactions on Signal Processing*, 48(6), 1737–1749. <https://doi.org/10.1109/78.845931>
- Pan, B., Duan, H. F., Meniconi, S., & Brunone, B. (2021). FRF-based transient wave analysis for the viscoelastic parameters identification and leak detection in water-filled plastic pipes. *Mechanical Systems and Signal Processing*, 146, 107056. <https://doi.org/10.1016/j.ymsp.2020.107056>
- Rezapour, Shafai Bejestan, M., & Aminnejad, B. (2021). Case study of leak detection based on Gaussian function in experimental viscoelastic water pipeline. *Water Supply*, 21(7), 3860–3874. <https://doi.org/10.2166/ws.2021.145>
- Sattar, A. M., & El-Beltagy, M. (2017). Stochastic solution to the water hammer equations using polynomial chaos expansion with random boundary and initial conditions. *Journal of Hydraulic Engineering*, 143(2), 04016078. [https://doi.org/10.1061/\(asce\)hy.1943-7900.0001227](https://doi.org/10.1061/(asce)hy.1943-7900.0001227)
- Soares, A. K., Covas, D. I. C., & Reis, L. F. R. (2011). Leak detection by inverse transient analysis in an experimental PVC pipe system. *Journal of Hydroinformatics*, 13(2), 153–166. <https://doi.org/10.2166/hydro.2010.012>
- Vitkovsky, J. P., Liggett, J., Simpson, A., & Lambert, M. (2003). Optimal measurement site locations for inverse transient analysis in pipe networks. *Journal of Water Resources Planning and Management*, 129(6), 480–492.
- Vitkovsky, J. P., Lambert, M. F., Simpson, A. R., & Liggett, J. A. (2007). Experimental observation and analysis of inverse transients for pipeline leak detection. *Journal of Water Resources Planning and Management*, 133(6), 519–530.
- Wang, G. (2018). Beam damage uncertainty quantification using guided Lamb wave responses. *Journal of Intelligent Material Systems and Structures*, 29(3), 323–334. <https://doi.org/10.1177/1045389X17704911>
- Wang, X. (2021). Uncertainty quantification and global sensitivity analysis for transient wave propagation in pressurized pipes. *Water Resources Research*, 57(4), e2020WR028975. <https://doi.org/10.1029/2020wr028975>
- Wang, X., & Ghidaoui, M. S. (2018). Identification of multiple leaks in pipeline: Linearized model, maximum likelihood, and super-resolution localization. *Mechanical Systems and Signal Processing*, 107, 529–548. <https://doi.org/10.1016/j.ymsp.2018.01.042>

- Wang, X., Lin, J., Keramat, A., Ghidaoui, M. S., Meniconi, S., & Brunone, B. (2019). Matched-field processing for leak localization in a viscoelastic pipe: An experimental study. *Mechanical Systems and Signal Processing*, *124*, 459–478. <https://doi.org/10.1016/j.ymssp.2019.02.004>
- Wang, X., Palomar, D. P., Zhao, L., Ghidaoui, M. S., & Murch, R. D. (2019). Spectral-based methods for pipeline leak detection. *Journal of Hydraulic Engineering, ASCE*, *145*(3), 04018089. [https://doi.org/10.1061/\(asce\)hy.1943-7900.0001572](https://doi.org/10.1061/(asce)hy.1943-7900.0001572)
- Wang, X., Waqar, M., Yan, H.-C., Louati, M., Ghidaoui, M. S., Lee, P. J., et al. (2020). Pipeline leak localization using matched-field processing incorporating prior information of modeling error. *Mechanical Systems and Signal Processing*, *143*, 106849. <https://doi.org/10.1016/j.ymssp.2020.106849>
- Wang, X.-J., Lambert, M. F., Simpson, A. R., Liggett, J. A., & Vítkovský, J. P. (2002). Leak detection in pipelines using the damping of fluid transients. *Journal of Hydraulic Engineering*, *128*(7), 697–711. [https://doi.org/10.1061/\(asce\)0733-9429\(2002\)128:7\(697\)](https://doi.org/10.1061/(asce)0733-9429(2002)128:7(697))
- Yue, & Aliabadi, M. (2020). Hierarchical approach for uncertainty quantification and reliability assessment of guided wave-based structural health monitoring. *Structural Health Monitoring*. <https://doi.org/10.1177/1475921720940642>
- Zanganeh, R., Jabbari, E., Tijsseling, A., & Keramat, A. (2020). Fluid-structure interaction in transient-based extended-defect detection of pipe walls. *Journal of Hydraulic Engineering, ASCE*, *146*(4). [https://doi.org/10.1061/\(asce\)hy.1943-7900.0001693](https://doi.org/10.1061/(asce)hy.1943-7900.0001693)
- Zhang, C., Gong, J., Lambert, M. F., Simpson, A. R., & Zecchin, A. C. (2019). Sensor placement strategy for pipeline condition assessment using inverse transient analysis. *Water Resources Management*, *33*(8), 2761–2774. <https://doi.org/10.1007/s11269-019-02239-2>
- Zhang, C., Lambert, M. F., Gong, J., Zecchin, A. C., Simpson, A. R., & Stephens, M. L. (2020). Bayesian inverse transient analysis for pipeline condition assessment: Parameter estimation and uncertainty quantification. *Water Resources Management*, *34*, 2807–2820. <https://doi.org/10.1007/s11269-020-02582-9>